The Astronomical Journal, 153:66 (26pp), 2017 February doi:10.3847/1538-3881/153/2/66

ROBO-AO *KEPLER* PLANETARY CANDIDATE SURVEY. III. ADAPTIVE OPTICS IMAGING OF 1629 *KEPLER* EXOPLANET CANDIDATE HOST STARS

Carl Ziegler[1], Nicholas M. Law[1], Tim Morton[2], Christoph Baranec[3], Reed Riddle[4], Dani Atkinson[3], Anna Baker[5], Sarah Roberts[6], and David R. Ciardi[7]
[1] Department of Physics and Astronomy, University of North Carolina at Chapel Hill, Chapel Hill, NC 27599-3255, USA; carlziegler@unc.edu
[2] Department of Astrophysical Sciences, Princeton University, Princeton, NJ 08544, USA
[3] Institute for Astronomy, University of Hawai'i at Mānoa, Hilo, HI 96720-2700, USA
[4] Division of Physics, Mathematics, and Astronomy, California Institute of Technology, Pasadena, CA 91125, USA
[5] Durham Academy Upper School, 3601 Ridge Road, Durham, NC 27705, USA
[6] Juniata College, 1700 Moore Street, Huntingdon, PA 16652, USA
[7] NASA Exoplanet Science Institute, California Institute of Technology, Pasadena, CA 91125, USA
Received 2016 May 11; revised 2016 September 6; accepted 2016 September 21; published 2017 January 13

ABSTRACT

The Robo-AO *Kepler* Planetary Candidate Survey is observing every *Kepler* planet candidate host star with laser adaptive optics imaging to search for blended nearby stars, which may be physically associated companions and/or responsible for transit false positives. In this paper, we present the results of our search for stars nearby 1629 *Kepler* planet candidate hosts. With survey sensitivity to objects as close as $\sim 0\farcs15$, and magnitude differences $\Delta m \leqslant 6$, we find 223 stars in the vicinity of 206 target KOIs; 209 of these nearby stars have not been previously imaged in high resolution. We measure an overall nearby-star probability for *Kepler* planet candidates of $12.6\% \pm 0.9\%$ at separations between $0\farcs15$ and $4\farcs0$. Particularly interesting KOI systems are discussed, including 26 stars with detected companions that host rocky, habitable zone candidates and five new candidate planet-hosting quadruple star systems. We explore the broad correlations between planetary systems and stellar binarity, using the combined data set of Baranec et al. and this paper. Our previous 2σ result of a low detected nearby star fraction of KOIs hosting close-in giant planets is less apparent in this larger data set. We also find a significant correlation between detected nearby star fraction and KOI number, suggesting possible variation between early and late *Kepler* data releases.

Key words: binaries: close – instrumentation: adaptive optics – methods: data analysis – methods: observational – planets and satellites: detection – techniques: high angular resolution

Supporting material: machine-readable table

1. INTRODUCTION

The primary *Kepler* mission vastly increased the tally of known extrasolar planets, discovering over 2300 confirmed planets and approximately 4700 planet candidates (Borucki et al. 2010, 2011a, 2011b; Batalha et al. 2013; Burke et al. 2014; Rowe et al. 2014; Thompson et al. 2015; Morton et al. 2016). Using high-precision photometry to detect the periodic dip in stellar brightness consistent with a transiting planet, *Kepler* exoplanet candidates (*Kepler* Objects of Interests, or KOIs) require follow-up observations to rule out astrophysical false positives and for host star characterization (Brown et al. 2011).

Most solar-type stars, which comprise the majority of *Kepler* targets (Batalha et al. 2013), form with at least one companion star (Duquennoy & Mayor 1991; Raghavan et al. 2010). The large effective point-spread function (PSF) ($6''$–$10''$) and coarse resolution (pixel size of $\sim 4''$) (Haas et al. 2010) of *Kepler* allow these companion stars and background objects to be blended with the host candidate, illustrated in Figure 1. High-angular-resolution follow-up imaging is crucial to distinguish these blended multiple stellar systems and identify false transit signals. Even when the candidates are bona fide planets, the planet radius measurements based on the diluted transit signal are underestimated, due to the presence of multiple stars in the system—or unbounded stars within the *Kepler* aperture (Ciardi et al. 2015).

Before being elevated to planet candidate status, each KOI is vetted for clear signatures of being an astrophysical false positive: center-of-light shifts during transit, an identifiable secondary eclipse signal indicating the eclipsing object is self-luminous, or sharing the exact ephemeris as another KOI. Although these vetting efforts on early catalogs were largely based on human inspection (Batalha et al. 2010), the most recent DR24 catalog has fully automated this process (Thompson et al. 2015). Notably, the candidate status of a KOI is *not* a function of its depth or shape (i.e., whether it is V-shaped), which means that a large fraction of the deeper signals ($\sim$50%) can be expected to be false positives (Santerne et al. 2012, 2016). Shallower candidates have a much lower predicted false positive rate ($\sim$10%) (Morton & Johnson 2011; Fressin et al. 2013), a prediction that has been confirmed by follow-up observations from the *Spitzer Space Telescope* (Désert et al. 2015). Nevertheless, even if a large fraction of the candidate signals are real planets, many of the inferred properties of these planets are affected by the presence of blended sources (Dressing & Charbonneau 2013; Santerne et al. 2013). Therefore, to fully characterize individual *Kepler* planets and to measure any possible biasing effects of stellar multiplicity on the planetary populations, every KOI needs to be searched for stellar companions.[8]

[8] For brevity, we denote stars which we found within our detection radius of KOIs as "companions," in the sense that they are asterisms associated on the sky.

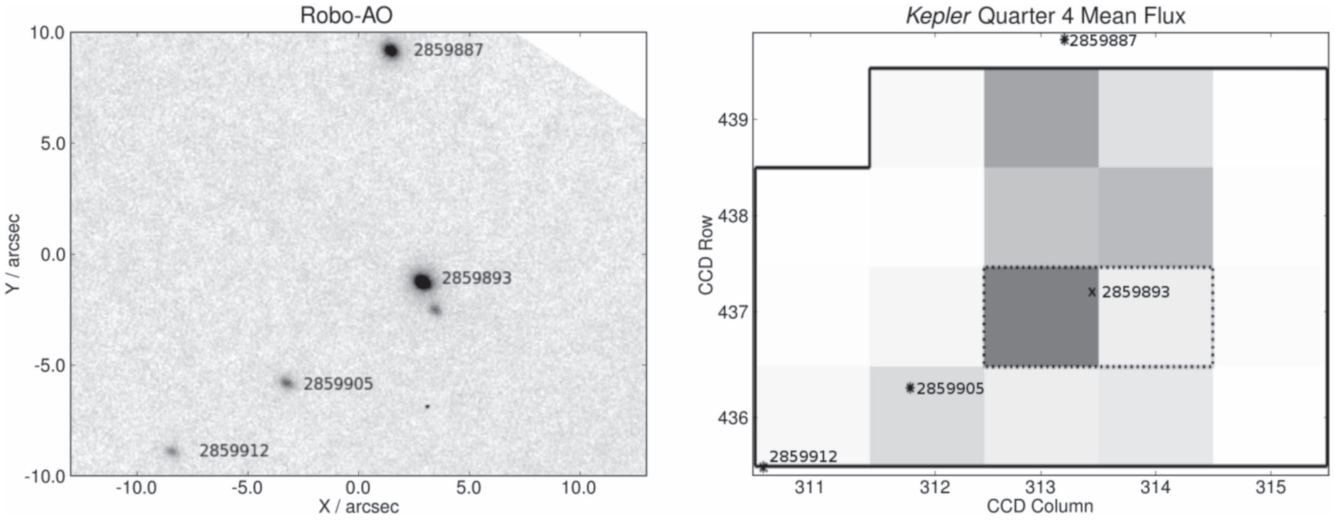

Figure 1. On the left, the full-frame Robo-AO reduced image of KOI-4418 (KIC2859893) rotated and scaled to match the *Kepler* view of the same field, displayed on the right, each pixel colored by the mean flux in Quarter 4. KICs in the field are marked on both images, as well as K_P magnitude in the *Kepler* image. The 1.″41 binary to KOI-4418 is not visible in the ∼4″ pixels of *Kepler*, illustrating how real companions and background stars can blend with the KOIs, resulting in astrophysical false positives or inaccurate planetary characteristics. High-resolution follow-ups are a crucial step in the validation and characterization of *Kepler* planetary systems.

There has been considerable effort by the community to perform high-resolution imaging surveys of the KOIs (Howell et al. 2011; Adams et al. 2012, 2013; Horch et al. 2012, 2014; Lillo-Box et al. 2012, 2014; Dressing et al. 2014; Marcy et al. 2014; Everett et al. 2015; Torres et al. 2015; Wang et al. 2015a, 2015b; Kraus et al. 2016). These surveys, however, have combined to cover approximately 30% of the full set of *Kepler* planetary candidates. This piecemeal approach leads to inconsistent vetting, while limiting the comprehensive statistics and correlations that can be derived from a large data set of high resolution images of multiple stellar systems hosting planetary systems. In addition, target lists of past surveys are often biased toward brighter targets, possibly skewing any interpretations drawn from the data.

A complete, consistent high-resolution survey of all the the KOIs with ground-based adaptive optics (AO) is limited by the typical overheads required with traditional systems. Taking advantage of the order-of-magnitude increase in time-efficiency provided by Robo-AO, the first robotic laser AO system, we are performing high-resolution imaging of every KOI system. The first paper in this survey, Law et al. (2014, hereafter Paper I) observed 715 *Kepler* planetary candidates, identifying 53 companions, with 43 new discoveries, for a detected companion fraction of 7.4% ± 1.0% within separations of 0.″15–2.″5. The second paper in this survey, Baranec et al. 2016, hereafter Paper II) observed 969 *Kepler* planetary candidates, identifying 202 companions, with 139 new discoveries, for a detected companion fraction of 11.0% ± 1.1% within separations of 0.″15–2.″5., and 18.1% ± 1.3% within separations of 0.″15–4.″0.

This paper presents a total of 1629 targets observed, around which we find 223 companions around 206 KOIs, 209 of which have not been previously imaged in high resolution, for a detected companion fraction of 12.6% ± 0.9% within 4.″0 of planetary candidate hosting stars.

We begin in Section 2 by describing our target selection, the Robo-AO system, and follow-up observations. In Section 3, we describe the Robo-AO data reduction and the companion detection and analysis. In Section 4, we describe the results of this survey, including discovered companions, and compare to other KOI surveys. We discuss the results in Section 5, detailing the effects on the planetary characteristics of the survey's discoveries and looking at the overall binarity statistics of the *Kepler* planet candidates. We conclude in Section 6.

2. SURVEY TARGETS AND OBSERVATIONS

2.1. Target Selection

KOI targets were selected from the KOI catalog based on Q1-Q17 *Kepler* data (Borucki et al. 2010, 2011a, 2011b; Batalha et al. 2013; Burke et al. 2014; Rowe et al. 2014; Thompson et al. 2015). We selected targets not observed in Papers I and II, with the objective of completing the Robo-AO survey of all KOIs, including those with already detected companions. Observations in this paper are primarily from the 2014–2015 observing seasons; residual observations of dim targets from 2012–2013 are also included—their analysis is now possible, using our improved binary detection and characterization pipeline. KOIs flagged as false positives using *Kepler* data were removed. In Figure 2, the properties of the targeted KOIs in this work, as well as for the full Robo-AO survey, as of the end of the 2015 observing season are compared to the set of all KOIs from Q1-Q17, with CANDIDATE dispositions based on *Kepler* data. The Robo-AO target distribution closely matches the full KOI list in magnitude, planetary radius, planetary orbital period, and stellar temperature. On-sky positions of all targeted KOIs in the complete survey are displayed in Figure 3.

2.2. Observations

2.2.1. Robo-AO

We obtained high-angular-resolution images of the 1629 KOIs during 55 separate nights of observations between 2012 July 16 and 2015 June 12 (UT), detailed in Table 9 in the Appendix. The observations were performed using the Robo-AO laser adaptive optics system (Riddle et al. 2012; Baranec et al. 2013, 2014b) mounted on the Palomar 1.5 m telescope. The first robotic laser guide star adaptive optics system, the automatic Robo-AO system can efficiently perform large, high

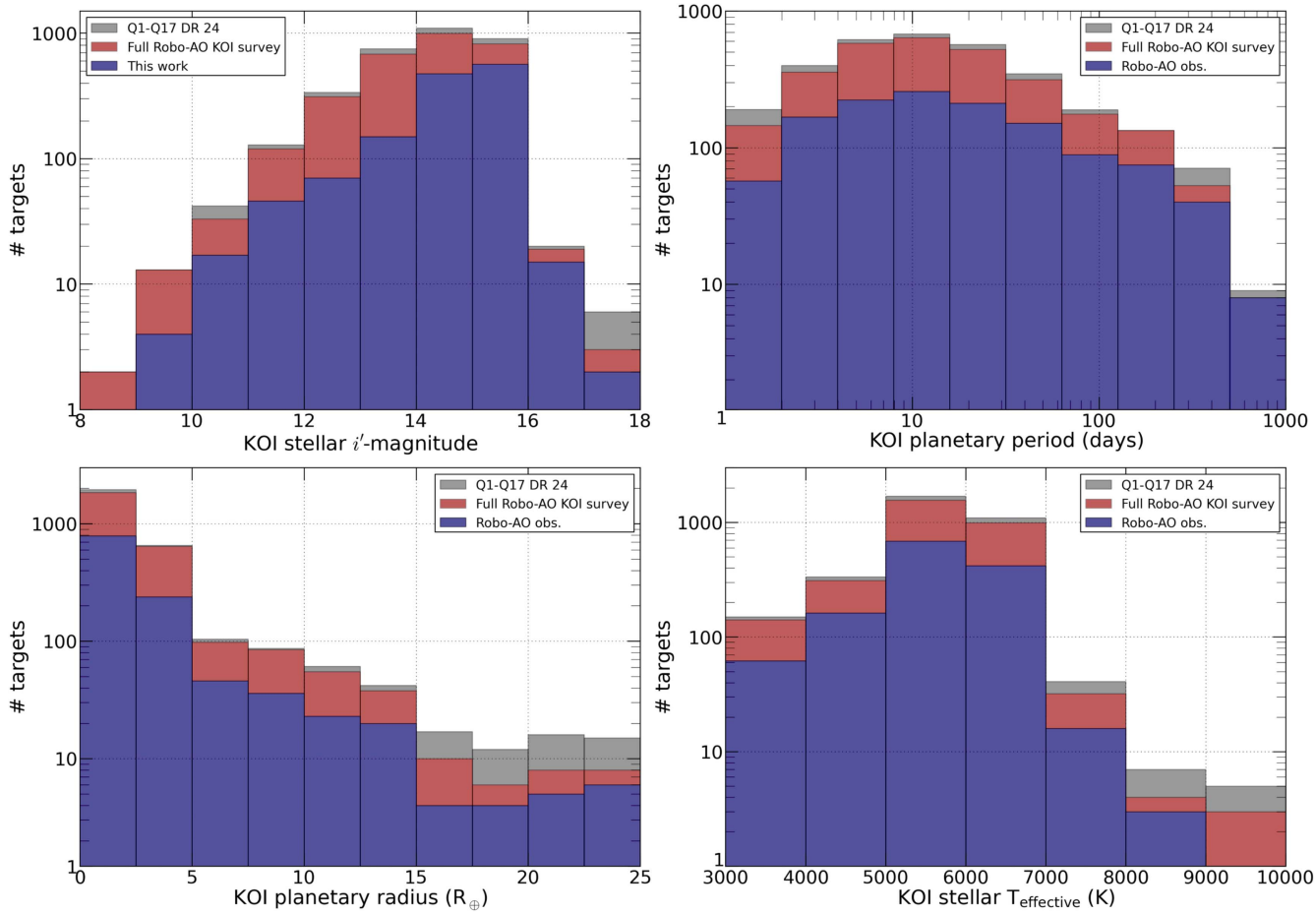

Figure 2. Comparison of the distribution of the Robo-AO sample in this paper as well as the combined Robo-AO survey (Papers I, II, and this work) to the complete set of KOIs from Q1-Q17 (Borucki et al. 2010, 2011a, 2011b; Batalha et al. 2013; Burke et al. 2014; Rowe et al. 2014; Thompson et al. 2015).

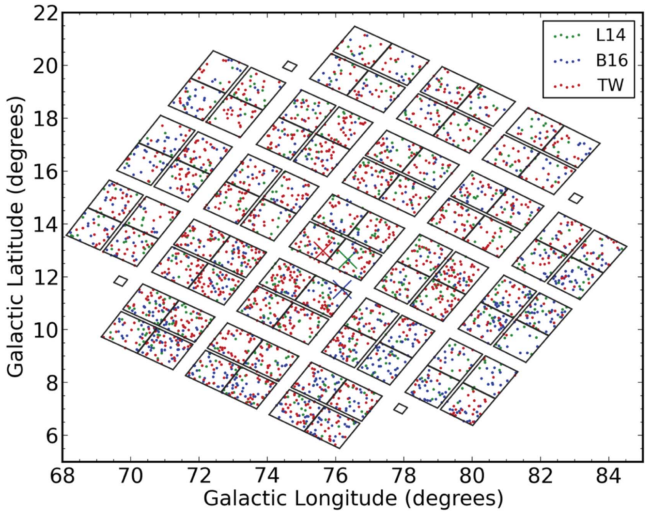

Figure 3. Location on sky of targeted KOIs from Paper I (L14), Paper II (B16), and this work (TW). The median coordinates of the targeted KOIs is designated by an "×". A projection of the *Kepler* field of view is provided for reference.

angular resolution surveys. The AO system runs at a loop rate of 1.2 kHz to correct high-order wavefront aberrations, delivering a median Strehl ratio of 9% in the i'-band. Observations were taken in either a i'-band filter or a long-pass filter cutting on at 600 nm (LP600 hereafter). The LP600 filter approximates the *Kepler* passband at redder wavelengths, while also suppressing blue wavelengths that reduce adaptive optics performance.

Table 1
Specifications of the Robo-AO KOI Survey

KOI targets	1629
FWHM resolution	∼0.″15 (@600–750 nm)
Observation wavelengths	600–950 nm
Field size	44″ × 44″
Detector format	1024^2 pixels
Pixel scale	43.1 mas/pix
Exposure time	90 s
Targets observed/hour	20
Observation dates	2012 July 16–2015 June 12

Typical seeing at the Palomar Observatory is between 0.″8 and 1.″8, with median around 1.″1 (Baranec et al. 2014b). The typical FWHM (diffraction limited) resolution of the Robo-AO system is 0.″15. Images are recorded on an electron-multiplying CCD (EMCCD), allowing short frame rates for tip and tilt correction in software using a natural guide star ($m_V < 16$) in the field of view. Specifications of the Robo-AO KOI survey are summarized in Table 1.

2.2.2. Keck LGS-AO

Eight candidate multiple systems were selected for re-imaging by the NIRC2 camera behind the Keck II laser guide

Table 2
Full Keck-AO Observation List

KOI	m_v	ObsID	Companion?	ΔK_p
1447	13.2	2015 Jul 25	yes	0.63 ± 0.06
1873	15.8	2015 Jul 25	⋯	⋯
2117	16.2	2015 Jul 25	yes	0.53 ± 0.06
2554	15.9	2015 Jul 25	yes	0.27 ± 0.05[a]
			yes	2.96 ± 0.10[b]
3020	13.8	2015 Jul 25	yes	1.27 ± 0.06[c]
			yes	5.01 ± 0.07[d]
3106	15.7	2015 Jul 25	yes	1.22 ± 0.13
5257	15.5	2015 Jul 25	⋯	⋯
5762	15.9	2015 Jul 25	yes	0.83 ± 0.08

Notes.
[a] Companion at $\rho = 0\farcs37$.
[b] New companion at $\rho = 3\farcs55$.
[c] Companion at $\rho = 0\farcs38$.
[d] New companion at $\rho = 3\farcs86$.

Table 3
Full Gemini Observation List

KOI	m_v	ObsID	Companion?	ΔK_p
327	13.1	2015 Aug 27	⋯	⋯
2198	12.8	2015 Aug 27	⋯	⋯
2833	12.8	2015 Aug 27	⋯	⋯
4131	13.2	2015 Jul 31	yes	4.41 ± 0.09[a]
			yes	4.96 ± 0.11[b]
4301	13.3	2015 Aug 27	⋯	⋯
5052	12.8	2015 Jul 31	yes	0.75 ± 0.04
5164	12.6	2015 Aug 27	⋯	⋯
5243	12.5	2015 Jul 31	yes	0.53 ± 0.05[c]
			yes	4.11 ± 0.09[d]
5497	11.0	2015 Aug 27	⋯	⋯
5774	11.1	2015 Aug 27	yes	1.54 ± 0.04

Notes.
[a] Companion at $\rho = 2\farcs85$.
[b] New companion at $\rho = 4\farcs24$.
[c] Companion at $\rho = 0\farcs77$.
[d] Companion at $\rho = 2\farcs41$.

star adaptive optics system (van Dam et al. 2006; Wizinowich et al. 2006), on 2015 July 25 (UT) to confirm possible companions. The targets were selected for their low significance of detectability, either because of low contrast ratio or small angular separation. Observations were performed in the $K_{\rm prime}$ filter using the narrow mode of NIRC2 (9.952 mas pixel^{-1}; Yelda et al. 2010), dithering the primary target at intervals of 30 s into the three lowest noise quadrants, for a total exposure time of 90 s. The images were corrected for geometric distortion using the NIRC2 distortion solution of Yelda et al. (2010). Targets observed with Keck are detailed in Table 2. Further follow-up observations of low-significance companion detections are ongoing and will appear in future papers in this survey.

2.2.3. Gemini LGS-AO

Seven candidate multiple systems from this work, and three from Papers I and II, again selected for their low detection significance, were re-imaged with the adaptive optics assisted NIRI instrument (Hodapp et al. 2003) on the Gemini North telescope. Three targets were observed on 2015 July 31 (UT) and seven targets were observed on 2015 August 27, using Band 3 allocated time. Targets observed with Gemini are detailed in Table 3. Observations were performed with the $F/32$ camera, providing resolution of 21.9 mas pixel^{-1} across a field of view of $22'' \times 22''$. Total integration times were 90 s in the $K_{\rm prime}$ band across three dithered images, used to increase dynamic range and allow sky subtraction. The common striping pattern found in NIRI images was removed using the *cleanir.py* script provided by the Gemini staff. The images were flat fielded, bad pixel corrected, and sky subtracted. The distortion solution provided by the Gemini staff was used to correct the images for distortion.

3. DATA REDUCTION

With the largest adaptive optics data set yet assembled by Robo-AO, the data reduction process was automated as much as possible for efficiency and consistency. As in Paper I and Ziegler et al. (2015), after initial pipeline reductions described in Section 3.1, the target stars were identified (Section 3.2), companions automatically identified (Section 3.5), PSF subtraction performed and companions again auto-identified (Section 3.4), and constraints of the companion sensitivity of the survey measured (Section 3.6). Finally, the properties of the detected companions are measured in Section 3.7.

3.1. Imaging Pipeline

The Robo-AO imaging pipeline (Law et al. 2009, 2014) reduced the images: the raw EMCCD output frames are dark-subtracted and flat-fielded and then stacked and aligned using the Drizzle algorithm (Fruchter & Hook 2002), which also up-samples the images by a factor of two. To avoid tip/tilt anisoplanatasism effects, the image motion was corrected by using the KOI itself as the guide star in each observation.

3.2. Target Verification

To verify that the star viewed in the image is the desired KOI target, we created Digital Sky Survey cutouts of similar angular size around the target coordinates. Each image was manually checked to assure no ambiguity in the target star with images with either poor performance or incorrect fields removed. These bad images made up approximately 2% of all our images, and for all but two of the targets, additional images were available.

3.3. Image Preparation

To facilitate the automation of the data reduction, centered $8\farcs5$ square cutouts were created around the 1629 verified target KOIs. We select a $4''$ separation cutoff for our companion search, in order to detect all nearby stars that would blend with the target KOI in a *Kepler* pixel.

3.4. PSF Subtraction

To identify close companions, a custom locally optimized PSF subtraction routine based on the Locally Optimized Combination of Images algorithm (Lafrenière et al. 2007) was applied to centered cutouts of all stars. Detailed in Paper I, the code uses a set of twenty KOI observations, selected from the observations within the same filter closest to the target observation in time, as reference PSFs, as it is improbable that a

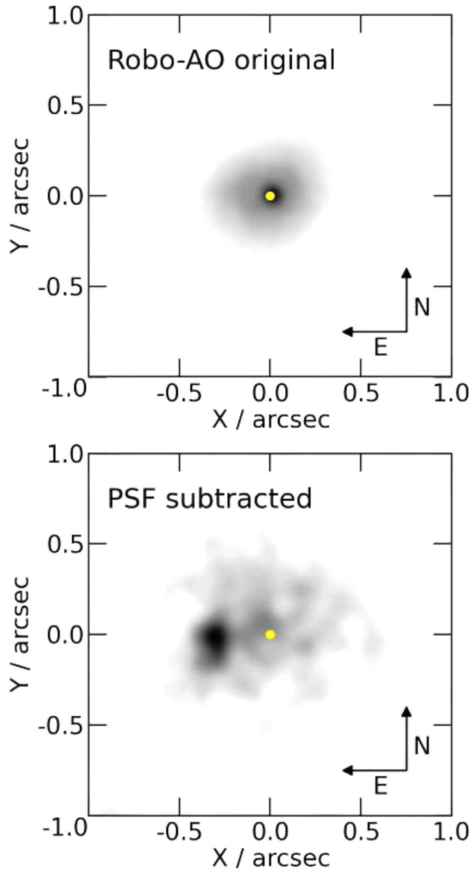

Figure 4. Example of PSF subtraction on KOI-5762 with companion separation of 0.″34. The yellow circle marks the position of the primary star's PSF peak. Both images have been scaled and smoothed for clarity. Successful removal of the PSF leaves residuals consistent with photon noise. The 2″ square field shown here is approximately equal to half the *Kepler* pixel size. The close companion to KOI-5762 was confirmed with NIRC2/Keck images, shown in Figure 7.

companion would appear at the same position in two different images. A locally optimized PSF is generated and subtracted from the original image, leaving residuals consistent with photon noise.

This procedure was performed on all KOI images out to 2″, and the results visually checked for companions. Figure 4 shows an example of the PSF subtraction performance. The PSF subtracted images were subsequently run through the automated companion finding routine, as described in Section 3.5.

3.5. Companion Detection

An initial visual companion search was performed redundantly by three of the authors. This search yielded a preliminary companion list, and filtered out bad images.

Continuing the companion search, we ran all images through a custom automated search algorithm, based on the code described in Paper I. The algorithm slides a 5-pixel diameter aperture within concentric annuli centered on the target star. Any aperture with $>+5\sigma$ outlier to the local noise is considered a potential astrophysical source. These are subsequently checked manually, eliminating spurious detections with dissimilar PSFs to the target star and those having characteristics of a cosmic ray hit, such as a single bright pixel or bright streak. The detection significance of "secure" companions are listed in Tables 4 and 5.

Many possible companions were visually identified but fell beneath the formal 5σ required for a discovery. Despite not reaching our formal significance level required for a discovery, previous results suggest that all but a small fraction are likely real: Keck/NIRC2 observations have confirmed all 15 "likely" detections in Paper I and all 38 re-observed "likely" companions in Paper II. The detection significance of these "likely" companions are listed in Tables 6 and 7.

3.6. Imaging Performance Metrics

The two dominant factors that affect the image performance of the Robo-AO system are seeing and target brightness. An automated routine was used to classify the image performance for each target. Described in detail in Paper I, the code uses PSF core size as a proxy for image performance. Observations were binned into three performance groups, with 31% fall in the low-performance group, 41% in the medium-performance group, and 28% in the high-performance group.

We determine the angular separation and contrast consistent with a 5σ detection by injecting artificial companions, a clone of the primary PSF. For concentric annuli of 0.″1 width, the detection limit is calculated by steadily dimming the artificial companion until the auto-companion detection algorithm (Section 3.5) fails to detect it. This process is subsequently performed at multiple random azimuths within each annulus, and the limiting 5σ magnitudes are averaged. For clarity, these average magnitudes for all radii measurements are fitted with functions of the form $a * \sin h(b * r + c) + d$ (where r is the radius from the target star and a, b, c and d are fitting variables). Contrast curves for the three performance groups are shown in Section 4 in Figure 5.

3.7. Companion Characterization

3.7.1. Contrast Ratios

For wide, resolved companions with little PSF overlap, the companion to primary star contrast ratio was determined using aperture photometry on the original images. The aperture radius was cycled in one-pixel increments from 1 to 5 FWHM for each system, with background measured opposite the primary from the companion (except in the few cases where another object falls near or within this region in the image). Photometric uncertainties are estimated from the standard deviation of the contrast ratios measured for the various aperture sizes.

For close companions, the estimated PSF was used to remove the blended contributions of each star before aperture photometry was performed. The locally optimized PSF subtraction algorithm can attempt to remove the flux from companions using other reference PSFs with excess brightness in those areas. For detection purposes, we use many PSF core sizes for optimization, and the algorithm's ability to remove the companion light is reduced. However, the companion is artificially faint as some flux has still been subtracted. To avoid this, the PSF fit was redone, excluding a six-pixel-diameter region around the detected companion. The large PSF regions allow the excess light from the primary star to be removed without reducing the brightness of the companion.

Table 4
Secure Detections of Objects within 2.″5 of *Kepler* Planet Candidates

KOI	$m_{i'}$ (mag)	ObsID	Filter	Det. Significance σ	Separation (″)	P.A. (°)	Mag. Diff. (mag)	Approx. Comp. Spectral Type[c]	Prev. High Res. Detection?	Prev. Low Res. Detection?	False Positive?[a]	N_{KOI}[b]
163	13.3	2012 Jul 18	LP600	17	1.22 ± 0.06	214 ± 2	–0.36 ± 0.03	K1	…	…	…	1
454	14.5	2014 Jul 16	LP600	6.6	1.49 ± 0.06	204 ± 2	2.08 ± 0.04	M0	…	…	…	1
510	14.3	2014 Jul 14	LP600	5.6	2.45 ± 0.06	348 ± 2	2.53 ± 0.05	M1	…	UKIRT	…	4
771	15.1	2014 Aug 27	LP600	18	1.77 ± 0.06	281 ± 2	0.94 ± 0.05	K5	W15	…	…	1
1137	13.8	2014 Jun 13	LP600	6.1	0.75 ± 0.06	197 ± 2	0.81 ± 0.08	K5	…	…	0.01	1
1409	15.0	2014 Jul 17	LP600	27	2.17 ± 0.06	312 ± 2	2.58 ± 0.02	M0	…	UKIRT	…	1
1447	13.0	2012 Sep 04	LP600	5.1	0.28 ± 0.03[d]	212 ± 2[d]	0.27 ± 0.08	F6	…	…	0.01, 0.02	2
1630	14.9	2014 Jul 16	LP600	12	1.77 ± 0.06	188 ± 2	0.91 ± 0.02	K3	…	UKIRT	…	1
1687	14.9	2014 Jul 17	LP600	6.3	2.11 ± 0.06	209 ± 2	4.10 ± 0.16	M5	…	…	…	1
1792	11.9	2014 Sep 02	LP600	9.6	1.99 ± 0.06	111 ± 2	0.98 ± 0.05	K4	CFOP	UKIRT	0.02	3
2091	15.5	2014 Aug 27	LP600	7.2	1.30 ± 0.06	215 ± 2	1.72 ± 0.04	M0	…	…	…	1
2093	15.2	2014 Aug 27	LP600	8.7	2.08 ± 0.06	352 ± 2	3.10 ± 0.02	M0	…	…	…	3
2163	14.4	2014 Aug 31	LP600	6.9	0.77 ± 0.06	248 ± 2	0.04 ± 0.03	G2	…	…	…	3
2535	14.6	2014 Aug 23	LP600	5.9	1.73 ± 0.06	21 ± 2	2.47 ± 0.02	M2	…	UKIRT	…	1
2554	15.0	2014 Sep 01	LP600	5.4	0.37 ± 0.03[d]	149 ± 2[d]	0.37 ± 0.08	M0	…	…	…	2
2813	13.3	2013 Aug 15	LP600	27	1.10 ± 0.06	258 ± 2	0.84 ± 0.02	K7	D14, K16	…	0.01	1
2896	11.9	2015 Jun 05	LP600	13	0.96 ± 0.06	272 ± 2	0.38 ± 0.02	F8	CFOP	…	0.01, 0.02	2
2900	15.0	2014 Sep 03	LP600	10	2.36 ± 0.06	85 ± 2	1.30 ± 0.04	M0	…	UKIRT	…	1
2976	15.6	2014 Aug 28	LP600	66	2.02 ± 0.06	198 ± 2	2.66 ± 0.06	M2	…	UKIRT	…	1
3020	13.5	2013 Aug 13	LP600	5.2	0.38 ± 0.03[d]	272 ± 2[d]	0.93 ± 0.22	G9	…	…	…	1
3042	15.8	2014 Aug 31	LP600	6.1	1.87 ± 0.06	147 ± 2	1.62 ± 0.02	K3	…	UKIRT	…	1
3112	15.6	2014 Sep 01	LP600	14	1.87 ± 0.06	151 ± 2	0.49 ± 0.03	K3	…	UKIRT	…	1
3120	14.6	2014 Aug 29	LP600	8.1	1.14 ± 0.06	278 ± 2	0.87 ± 0.03	G8	…	…	…	1
3214	11.8	2014 Aug 29	LP600	10	1.41 ± 0.06	198 ± 2	2.50 ± 0.04	M0	…	…	…	2
3413	15.0	2014 Aug 26	LP600	54	2.18 ± 0.06	12 ± 2	3.79 ± 0.03	M2	…	UKIRT	0.01	1
3415	13.1	2013 Jul 27	LP600	10	0.74 ± 0.06	89 ± 2	0.03 ± 0.05	G9	…	…	…	1
3483	14.7	2014 Nov 09	LP600	11	1.51 ± 0.06	23 ± 2	2.15 ± 0.03	K5	…	…	…	1
3649	15.2	2014 Aug 23	LP600	8.1	0.79 ± 0.06	216 ± 2	0.26 ± 0.03	F9	LB14	…	0.01	1
3660	15.3	2014 Aug 24	LP600	6.5	0.60 ± 0.06	160 ± 2	1.05 ± 0.12	K4	…	…	…	1
3770	13.9	2014 Jun 19	LP600	11	1.20 ± 0.06	34 ± 2	1.44 ± 0.04	K1	…	…	…	1
3886	9.5	2014 Aug 20	i'	13	0.50 ± 0.06	116 ± 2	1.13 ± 0.09	M0	LB14	…	0.01	1
4343	13.5	2014 Jun 19	LP600	9.2	0.89 ± 0.06	138 ± 2	1.13 ± 0.05	M4	…	…	…	1
4418	15.7	2014 Sep 03	LP600	5.3	1.41 ± 0.06	172 ± 2	2.23 ± 0.02	M0	…	…	…	1
4550	15.0	2014 Aug 29	LP600	15	1.03 ± 0.06	325 ± 2	0.04 ± 0.02	K4	…	UKIRT	…	1
4713	13.4	2014 Jul 16	LP600	39	1.72 ± 0.06	251 ± 2	0.27 ± 0.04	G7	…	UKIRT	…	1
4750	15.7	2014 Aug 29	LP600	124	2.09 ± 0.06	322 ± 2	1.95 ± 0.02	M0	…	UKIRT	…	1
4895	14.5	2014 Aug 31	LP600	5.8	2.27 ± 0.06	75 ± 2	2.28 ± 0.02	M0	…	UKIRT	…	2
5004	14.3	2014 Jul 16	LP600	6.4	1.05 ± 0.06	109 ± 2	1.05 ± 0.02	K3	…	…	…	1
5052	12.5	2014 Jun 17	LP600	6.0	0.75 ± 0.06	285 ± 2	0.68 ± 0.06	F6	…	…	…	1
5243	12.2	2014 Sep 03	LP600	11	0.77 ± 0.06	17 ± 2	0.55 ± 0.03	G4	…	…	0.01	1
5243	12.2	2014 Sep 03	LP600	7.2	2.41 ± 0.06	128 ± 2	5.53 ± 0.08	M4	…	UKIRT	0.01	1
5570	14.5	2014 Aug 21	LP600	7.7	2.06 ± 0.06	236 ± 2	4.64 ± 0.06	M4	…	…	…	1
5578	10.9	2014 Nov 09	LP600	7.4	0.33 ± 0.06	89 ± 2	1.78 ± 0.22	K7	CFOP	…	…	1
5665	11.3	2014 Jul 17	LP600	106	2.11 ± 0.06	91 ± 2	3.24 ± 0.03	M1	CFOP	…	…	1
5671	13.4	2014 Jun 16	LP600	61	2.17 ± 0.06	225 ± 2	1.79 ± 0.05	K4	…	UKIRT	…	1
5774	10.7	2014 Sep 01	LP600	19	1.32 ± 0.06	336 ± 2	1.90 ± 0.05	G8	…	…	0.01	1
5889	15.2	2014 Sep 01	LP600	5.6	0.77 ± 0.06	246 ± 2	1.42 ± 0.11	K1	…	…	0.01	1

Table 4
(Continued)

KOI	$m_{i'}$ (mag)	ObsID	Filter	Det. Significance σ	Separation ($''$)	P.A. ($^\circ$)	Mag. Diff. (mag)	Approx. Comp. Spectral Type[c]	Prev. High Res. Detection?	Prev. Low Res. Detection?	False Positive?[a]	$N_{\rm KOI}$[b]
6111	12.9	2015 Jun 04	LP600	8.7	2.14 ± 0.06	48 ± 2	4.40 ± 0.05	M1	⋯	⋯	⋯	1
6132	14.6	2015 Jun 12	LP600	6.7	1.23 ± 0.06	91 ± 2	0.90 ± 0.03	G8	⋯	⋯	⋯	3
6258	11.2	2015 Jun 04	LP600	9.5	2.17 ± 0.06	241 ± 2	4.14 ± 0.14	M2	CFOP	⋯	0.01	1
6329	14.0	2015 Jun 04	LP600	6.2	1.22 ± 0.06	279 ± 2	1.43 ± 0.06	K2	⋯	⋯	⋯	1
6415	14.0	2015 Jun 03	LP600	5.9	1.75 ± 0.06	48 ± 2	1.17 ± 0.04	K5	⋯	UKIRT	⋯	1
6475	13.7	2015 Jun 07	LP600	14	1.31 ± 0.06	57 ± 2	0.50 ± 0.02	M2	⋯	⋯	⋯	1
6482	13.6	2015 Jun 04	LP600	5.8	0.52 ± 0.06	271 ± 2	0.58 ± 0.07	G7	⋯	⋯	0.01	1
6527	12.3	2015 Jun 07	LP600	224	2.21 ± 0.06	353 ± 2	1.60 ± 0.02	G7	CFOP	⋯	0.01	1
6560	12.9	2015 Jun 06	LP600	28	2.20 ± 0.06	30 ± 2	5.38 ± 0.07	M5	⋯	⋯	0.01	1
7205	14.1	2015 Jun 04	LP600	6.0	1.04 ± 0.06	42 ± 2	0.44 ± 0.03	G8	⋯	⋯	⋯	1
7448	11.3	2015 Jun 12	LP600	12	0.87 ± 0.06	260 ± 2	1.40 ± 0.09	G0	⋯	⋯	0.01	1

Notes. References for previous detections are denoted using the following codes: Dressing et al. 2014 (D14), Lillo-Box et al. 2014 (LB14), Kraus et al. 2016 (K16), Wang et al. 2015a (W15), visible in United Kingdom InfraRed Telescope images (UKIRT), high angular resolution images available on *Kepler* Community FollowUp Observing Program (CFOP).

[a] Probability that planetary transit signal is a false positive based on *Kepler* data.

[b] Number of planet candidates detected orbiting KOI.

[c] Estimation method described in Section 3.7.3.

[d] From Keck follow-up, described in Section 4.

Table 5
Secure Detections of Objects Outside 2.″5 and within 4.″0 of *Kepler* Planet Candidates

KOI	$m_{i'}$ (mag)	ObsID	Filter	Det. Significance σ	Separation (″)	P.A. (°)	Mag. Diff. (mag)	Approx. Comp. Spectral Type[c]	Prev. High Res. Detection?	Prev. Low Res. Detection?	False Positive?[a]	N_{KOI}[b]
255	14.5	2014 Jul 17	LP600	5.8	3.41 ± 0.06	357 ± 2	2.14 ± 0.04	M4	K16	UKIRT	⋯	2
734	15.1	2014 Sep 02	LP600	6.3	3.51 ± 0.06	175 ± 2	2.05 ± 0.04	K7	⋯	UKIRT	⋯	2
1558	15.0	2014 Jul 11	LP600	6.2	3.61 ± 0.06	308 ± 2	1.09 ± 0.04	K0	⋯	J19401085+4658310	0.01	1
1593	15.6	2014 Aug 24	LP600	7.6	3.24 ± 0.06	80 ± 2	1.60 ± 0.03	K4	⋯	UKIRT	⋯	2
1846	15.5	2014 Sep 02	LP600	5.2	3.77 ± 0.06	136 ± 2	1.07 ± 0.03	K7	⋯	J19192894+4643440	⋯	1
2213	15.1	2014 Aug 24	LP600	7.1	3.94 ± 0.06	91 ± 2	1.67 ± 0.02	M0	⋯	J19411432+4302399	⋯	1
2744	14.9	2014 Jul 17	LP600	5.7	3.50 ± 0.06	257 ± 2	2.12 ± 0.03	M0	⋯	UKIRT	⋯	2
3791	13.6	2014 Aug 22	i'	7.9	3.50 ± 0.06	258 ± 2	1.89 ± 0.04	K3	⋯	UKIRT	⋯	2
3928	13.1	2014 Jul 14	LP600	21	2.96 ± 0.06	265 ± 2	1.21 ± 0.03	G6	⋯	UKIRT	⋯	1
4343	13.5	2014 Jun 19	LP600	6.1	3.68 ± 0.06	350 ± 2	4.81 ± 0.15	M3	⋯	UKIRT	⋯	1
4630	14.7	2014 Jul 17	LP600	6.6	3.94 ± 0.06	53 ± 2	2.17 ± 0.05	M0	⋯	J19422364+4335492	⋯	1
4743	14.7	2014 Sep 03	LP600	7.9	3.06 ± 0.06	98 ± 2	2.29 ± 0.04	M0	⋯	UKIRT	0.01	1
4993	12.5	2014 Sep 01	LP600	8.8	3.49 ± 0.06	148 ± 2	4.13 ± 0.02	M2	⋯	UKIRT	⋯	1
5220	11.8	2014 Sep 03	LP600	29	2.89 ± 0.06	216 ± 2	3.27 ± 0.05	M3	⋯	UKIRT	⋯	1
5327	15.0	2014 Sep 01	LP600	31	3.96 ± 0.06	342 ± 2	–0.12 ± 0.03	M1	⋯	J19261347+4212546	⋯	1
5332	14.3	2015 Jun 12	LP600	15	3.61 ± 0.06	129 ± 2	0.63 ± 0.03	G7	⋯	J19405741+4219181	⋯	1
5465	13.7	2014 Jun 19	LP600	19	2.85 ± 0.06	158 ± 2	1.36 ± 0.05	K3	⋯	UKIRT	⋯	1
7020	13.5	2015 Jun 12	LP600	14	3.28 ± 0.06	23 ± 2	1.43 ± 0.04	G9	⋯	UKIRT	0.01	1
7395	11.7	2015 Jun 12	LP600	9.0	3.41 ± 0.06	212 ± 2	3.00 ± 0.04	G8	CFOP	UKIRT	0.01	1

Notes. References for previous detections are denoted using the following codes: Kraus et al. 2016 (K16), visible in United Kingdom InfraRed Telescope images (UKIRT), high angular resolution images available on *Kepler* Community FollowUp Observing Program (CFOP), companions visible in UKIRT and with 2MASS designations (J*).

[a] Probability that planetary transit signal is a false positive based on *Kepler* data.

[b] Number of planet candidates detected orbiting KOI.

[c] Estimation method described in Section 3.7.3.

Table 6
Likely Detections of Objects within 2.″5 of *Kepler* Planet Candidates

KOI	$m_{i'}$ (mag)	ObsID	Filter	Det. Significance σ	Separation (″)	P.A. (°)	Mag. Diff. (mag)	Approx. Comp. Spectral Type[c]	Prev. High Res. Detection?	Prev. Low Res. Detection?	False Positive?[a]	N_{KOI}[b]
126	13.1	2015 Jun 08	LP600	3.3	0.34 ± 0.06	36 ± 2	0.97 ± 0.15	K1	⋯	⋯	0.01, 0.02	2
200	14.2	2014 Sep 01	LP600	3.0	0.30 ± 0.06	44 ± 2	0.52 ± 0.23	G7	⋯	⋯	⋯	1
225	14.6	2014 Jul 16	LP600	3.5	0.53 ± 0.06	338 ± 2	0.93 ± 0.15	G8	⋯	⋯	0.01	1
532	14.5	2014 Jul 17	LP600	2.8	0.97 ± 0.06	232 ± 2	3.44 ± 0.25	M1		⋯	⋯	1
841	15.8	2012 Sep 02	LP600	2.6	2.00 ± 0.06	69 ± 2	3.60 ± 0.04	M3	LB12	⋯	⋯	5
1261	14.9	2014 Aug 22	i'	2.9	1.83 ± 0.06	340 ± 2	1.58 ± 0.05	K3	⋯	UKIRT	⋯	2
1503	14.6	2014 Aug 22	i'	3.1	0.77 ± 0.06	107 ± 2	1.52 ± 0.16	M0	⋯	⋯	⋯	1
1506	14.8	2014 Sep 02	LP600	2.8	1.15 ± 0.06	14 ± 2	3.14 ± 0.16	M1	⋯	⋯	⋯	1
1656	14.8	2014 Jun 13	LP600	4.5	1.06 ± 0.06	189 ± 2	1.65 ± 0.09	K4	⋯	⋯	⋯	1
1660	15.4	2014 Aug 28	LP600	2.7	1.40 ± 0.06	23 ± 2	2.00 ± 0.08	K7	⋯	⋯	⋯	1
1695	13.6	2014 Aug 31	LP600	2.8	0.31 ± 0.06	215 ± 2	0.61 ± 0.26	G7	⋯	⋯	⋯	1
1792	11.9	2014 Sep 02	LP600	3.7	0.53 ± 0.06	284 ± 2	1.06 ± 0.16	K4	CFOP	⋯	0.02	3
1908	14.2	2014 Aug 22	i'	4.2	1.29 ± 0.06	260 ± 2	4.11 ± 0.13	M5	K16		⋯	2
1973	15.3	2014 Aug 28	LP600	3.7	0.79 ± 0.06	31 ± 2	1.69 ± 0.19	M2	⋯	⋯	⋯	1
2048	15.5	2014 Aug 28	LP600	2.9	1.84 ± 0.06	353 ± 2	3.33 ± 0.17	M4	⋯	UKIRT	0.02	2
2117	15.2	2014 Nov 09	LP600	4.9	0.33 ± 0.03[d]	111 ± 2[d]	0.71 ± 0.17	M0	⋯	⋯	⋯	1
2283	14.7	2014 Sep 01	LP600	3.5	1.05 ± 0.06	21 ± 2	1.46 ± 0.10	M2	⋯	⋯	0.01	1
2376	15.0	2014 Aug 21	LP600	3.1	0.40 ± 0.06	213 ± 2	0.46 ± 0.12	K4	⋯	⋯	⋯	1
2445	15.6	2014 Aug 28	LP600	4.9	2.10 ± 0.06	25 ± 2	3.21 ± 0.03	M2	⋯	UKIRT	⋯	1
2460	14.6	2014 Aug 29	LP600	3.3	2.36 ± 0.06	192 ± 2	3.41 ± 0.02	M4	⋯	UKIRT	⋯	1
2482	14.8	2014 Aug 24	LP600	3.2	0.31 ± 0.06	212 ± 2	0.59 ± 0.28	G9	⋯	⋯	⋯	1
2580	15.5	2014 Aug 31	LP600	4.2	0.60 ± 0.06	154 ± 2	0.86 ± 0.13	K4	⋯	⋯	⋯	1
2688	16.1	2014 Aug 31	LP600	3.6	1.09 ± 0.06	205 ± 2	0.86 ± 0.04	M0	⋯	⋯	⋯	1
2760	14.5	2014 Aug 23	LP600	3.7	0.45 ± 0.06	142 ± 2	0.84 ± 0.16	M0	⋯	⋯	⋯	1
2797	15.6	2014 Aug 28	LP600	2.6	0.35 ± 0.06	222 ± 2	0.72 ± 0.25	G7	⋯	⋯	⋯	1
2851	15.2	2014 Aug 26	LP600	3.1	0.39 ± 0.06	223 ± 2	0.45 ± 0.08	K2	⋯	⋯	⋯	2
2856	15.1	2014 Aug 26	LP600	3.6	2.31 ± 0.06	287 ± 2	3.44 ± 0.03	M1	⋯	UKIRT	⋯	1
2862	15.3	2014 Aug 27	LP600	3.0	0.68 ± 0.06	20 ± 2	0.17 ± 0.05	M2	⋯	⋯	⋯	1
2926	15.7	2014 Aug 28	LP600	3.4	0.33 ± 0.06	16 ± 2	0.27 ± 0.09	M1	⋯	⋯	⋯	4
2927	15.7	2014 Aug 28	LP600	3.5	1.39 ± 0.06	36 ± 2	2.65 ± 0.04	M0	⋯	⋯	⋯	1
2958	14.6	2014 Sep 02	LP600	2.3	1.15 ± 0.06	302 ± 2	2.47 ± 0.14	K7	⋯	⋯	⋯	1
3043	14.6	2014 Jul 12	LP600	3.2	1.14 ± 0.06	68 ± 2	1.94 ± 0.07	K5	⋯	⋯	⋯	2
3106	15.2	2014 Aug 26	LP600	3.0	0.30 ± 0.03[d]	189 ± 2[d]	0.76 ± 0.16	G9	⋯	⋯	⋯	1
3136	15.4	2014 Aug 28	LP600	4.5	1.83 ± 0.06	238 ± 2	2.91 ± 0.04	M3	⋯	⋯	⋯	1
3214	11.8	2014 Aug 29	LP600	3.2	0.49 ± 0.06	320 ± 2	0.73 ± 0.13	G8	CFOP	⋯	⋯	2
3263	15.3	2014 Aug 23	LP600	3.0	0.80 ± 0.06	276 ± 2	2.01 ± 0.16	M5	LB14	⋯	0.01	1
3335	15.6	2014 Sep 01	LP600	3.3	2.40 ± 0.06	61 ± 2	2.89 ± 0.04	M0	⋯	UKIRT	⋯	1
3372	15.2	2014 Aug 23	LP600	4.3	2.36 ± 0.06	127 ± 2	1.95 ± 0.02	K5	⋯	UKIRT	⋯	1
3418	15.2	2014 Aug 23	LP600	3.9	1.13 ± 0.06	43 ± 2	1.29 ± 0.10	K2	⋯	⋯	⋯	1
3432	14.8	2014 Jul 16	LP600	2.8	0.66 ± 0.06	113 ± 2	1.37 ± 0.17	M0	⋯	⋯	⋯	1
3471	13.0	2014 Jul 11	LP600	2.9	0.63 ± 0.06	224 ± 2	3.05 ± 0.12	M3	CFOP	⋯	0.01	1
3480	15.7	2014 Sep 03	LP600	3.6	0.40 ± 0.06	210 ± 2	0.75 ± 0.20	K4	⋯	⋯	⋯	1
3611	16.3	2014 Aug 26	LP600	3.1	2.30 ± 0.06	267 ± 2	2.77 ± 0.05	M0	⋯	⋯	⋯	1
3626	16.2	2014 Sep 03	LP600	4.3	1.96 ± 0.06	310 ± 2	3.82 ± 0.14	M2	⋯	UKIRT	0.01	1
3783	12.8	2014 Aug 21	LP600	4.9	1.13 ± 0.06	272 ± 2	3.53 ± 0.15	K5	CFOP		0.01	1
4062	13.9	2014 Aug 29	LP600	3.4	1.49 ± 0.06	28 ± 2	3.66 ± 0.13	M0	⋯	⋯	0.01	1
4267	15.0	2014 Jun 19	LP600	3.9	1.66 ± 0.06	194 ± 2	3.29 ± 0.08	M0	⋯	⋯	⋯	1

Table 6
(Continued)

KOI	$m_{i'}$ (mag)	ObsID	Filter	Det. Significance σ	Separation ($''$)	P.A. (°)	Mag. Diff. (mag)	Approx. Comp. Spectral Type[c]	Prev. High Res. Detection?	Prev. Low Res. Detection?	False Positive?[a]	N_{KOI}[b]
4323	13.4	2014 Jun 13	LP600	3.8	1.12 ± 0.06	96 ± 2	2.22 ± 0.10	K5	⋯	⋯	0.02	2
4366	15.3	2014 Aug 28	LP600	2.7	2.46 ± 0.06	303 ± 2	3.38 ± 0.02	M3	⋯	⋯	⋯	1
4421	12.6	2014 Jul 12	LP600	3.4	2.45 ± 0.06	322 ± 2	4.62 ± 0.02	M3	⋯	UKIRT	⋯	2
4549	15.7	2014 Aug 27	LP600	3.0	0.75 ± 0.06	149 ± 2	1.99 ± 0.14	K7	⋯	⋯	⋯	1
4590	15.5	2014 Sep 02	LP600	4.8	0.87 ± 0.06	340 ± 2	0.38 ± 0.03	K3	⋯	⋯	⋯	1
4653	13.4	2014 Jul 19	LP600	2.7	0.77 ± 0.06	324 ± 2	2.02 ± 0.24	K3	⋯	⋯	⋯	1
4759	14.8	2014 Jul 19	LP600	2.6	0.67 ± 0.06	4 ± 2	2.12 ± 0.28	K7	⋯	⋯	⋯	1
4810	15.0	2014 Aug 24	LP600	3.0	2.36 ± 0.06	146 ± 2	3.16 ± 0.03	M1	⋯	UKIRT	⋯	1
4923	13.0	2014 Jul 14	LP600	4.7	0.78 ± 0.06	123 ± 2	1.46 ± 0.10	K2	⋯	⋯	⋯	1
4974	15.5	2014 Aug 26	LP600	2.9	1.23 ± 0.06	242 ± 2	3.33 ± 0.13	M2	⋯	⋯	⋯	1
5101	12.9	2014 Jul 17	LP600	3.1	1.24 ± 0.06	99 ± 2	3.33 ± 0.19	M0	⋯	⋯	⋯	1
5143	15.7	2014 Nov 09	LP600	3.8	1.22 ± 0.06	222 ± 2	3.83 ± 0.18	M3	⋯	⋯	⋯	1
5232	13.5	2014 Aug 31	LP600	4.0	1.75 ± 0.06	200 ± 2	4.67 ± 0.19	M2	⋯	⋯	⋯	1
5327	15.0	2014 Sep 01	LP600	4.8	1.88 ± 0.06	211 ± 2	3.43 ± 0.05	M5	⋯	⋯	⋯	1
5332	14.3	2015 Jun 12	LP600	4.1	2.19 ± 0.06	7 ± 2	2.37 ± 0.04	K7	⋯	UKIRT	⋯	1
5340	15.0	2014 Jun 19	LP600	3.0	1.24 ± 0.06	217 ± 2	2.66 ± 0.17	M0	⋯	⋯	⋯	1
5373	11.5	2015 Jun 05	LP600	3.1	0.21 ± 0.06	81 ± 2	0.12 ± 0.03	K3	⋯	⋯	⋯	1
5440	15.1	2014 Aug 28	LP600	3.2	2.45 ± 0.06	345 ± 2	3.04 ± 0.02	M0	⋯	UKIRT	⋯	1
5482	15.0	2014 Aug 31	LP600	3.6	0.62 ± 0.06	270 ± 2	1.44 ± 0.18	K2	⋯	⋯	0.01	1
5486	12.6	2015 Jun 12	LP600	2.9	0.34 ± 0.06	333 ± 2	0.73 ± 0.28	F6		⋯	⋯	1
5553	15.3	2014 Aug 23	LP600	3.3	0.97 ± 0.06	346 ± 2	2.52 ± 0.18	M1	⋯	⋯	⋯	1
5695	14.9	2015 Jun 12	LP600	3.0	0.60 ± 0.06	163 ± 2	1.47 ± 0.20	K2	⋯	⋯	0.01	1
5762	15.4	2014 Sep 03	LP600	3.7	0.23 ± 0.03[d]	95 ± 2[d]	0.65 ± 0.25	K3	⋯	⋯	⋯	1
6109	11.9	2015 Jun 07	LP600	4.6	0.60 ± 0.06	322 ± 2	1.30 ± 0.17	G6	CFOP	⋯	0.01,0.02	2
6202	11.4	2014 Aug 23	i'	2.9	0.77 ± 0.06	322 ± 2	2.49 ± 0.27	M2	⋯	⋯	⋯	1
6311	9.0	2015 Jun 04	LP600	3.1	1.75 ± 0.06	290 ± 2	0.83 ± 0.10	F3	⋯	⋯	0.01	1
6464	13.7	2015 Jun 04	LP600	3.9	0.75 ± 0.06	122 ± 2	1.72 ± 0.15	K0	⋯		0.01,0.02,0.03	3
6483	12.5	2015 Jun 05	LP600	3.2	1.41 ± 0.06	272 ± 2	2.78 ± 0.14	M0	⋯		0.01	1
6539	12.5	2015 Jun 12	LP600	3.1	1.58 ± 0.06	175 ± 2	3.89 ± 0.17	K7	⋯		0.01	1
6602	10.2	2015 Jun 03	LP600	4.8	0.77 ± 0.06	322 ± 2	0.54 ± 0.05	K4	⋯	⋯	0.01	1
6610	15.3	2015 Jun 12	LP600	4.0	1.73 ± 0.06	84 ± 2	2.68 ± 0.04	K3	⋯	⋯	⋯	1
6654	13.5	2015 Jun 12	LP600	3.9	1.41 ± 0.06	195 ± 2	2.88 ± 0.08	K7	⋯	⋯	0.01	1
6706	13.8	2015 Jun 04	LP600	3.0	1.04 ± 0.06	339 ± 2	1.44 ± 0.10	G6	⋯	⋯	0.01	1
6728	13.9	2015 Jun 12	LP600	3.3	1.94 ± 0.06	134 ± 2	5.04 ± 0.11	M4	⋯	⋯	⋯	1
7426	15.4	2015 Jun 05	LP600	3.2	2.45 ± 0.06	212 ± 2	2.37 ± 0.02	M2	⋯	UKIRT	⋯	1

Notes. References for previous detections are denoted using the following codes: Lillo-Box et al. 2012 (LB12), Lillo-Box et al. 2014 (LB14), Kraus et al. 2016 (K16), visible in United Kingdom InfraRed Telescope images (UKIRT).

[a] Probability that planetary transit signal is a false positive based on *Kepler* data.

[b] Number of planet candidates detected orbiting KOI.

[c] Estimation method described in Section 3.7.3.

[d] From Keck follow-up, described in Section 4.

Table 7
Likely Detections of Objects Outside 2.″5 and within 4.″0 of *Kepler* Planet Candidates

KOI	m_i' (mag)	ObsID	Filter	Det. Significance σ	Separation (″)	P.A. (°)	Mag. Diff. (mag)	Approx. Comp. Spectral Type[c]	Prev. High Res. Detection?	Prev. Low Res. Detection?	False Positive?[a]	N_{KOI}[b]
51	13.4	2013 Jul 25	LP600	2.6	3.51 ± 0.06	161 ± 2	2.63 ± 0.07	M0	⋯	⋯	⋯	1
193	14.7	2014 Aug 21	LP600	4.8	2.78 ± 0.06	137 ± 2	3.07 ± 0.02	M0	⋯	UKIRT	0.01	1
200	14.2	2014 Sep 01	LP600	3.8	2.81 ± 0.06	130 ± 2	4.00 ± 0.02	M2	⋯	UKIRT	⋯	1
240	14.8	2014 Aug 21	LP600	4.2	2.71 ± 0.06	272 ± 2	3.46 ± 0.03	M1	⋯	UKIRT	⋯	1
326	13.0	2013 Aug 15	LP600	4.9	3.53 ± 0.06	267 ± 2	2.01 ± 0.02	M2	LB12	⋯	⋯	2
541	14.5	2014 Aug 29	LP600	4.5	2.80 ± 0.06	246 ± 2	3.50 ± 0.02	M3	⋯	UKIRT	⋯	1
598	14.5	2014 Jul 11	LP600	4.3	3.17 ± 0.06	357 ± 2	2.73 ± 0.04	M2	⋯	UKIRT	0.02	2
757	15.5	2014 Sep 03	LP600	3.7	2.94 ± 0.06	243 ± 2	3.37 ± 0.04	M3	⋯	J19244737+4718244	0.02	3
814	15.3	2014 Aug 24	LP600	2.7	3.40 ± 0.06	346 ± 2	4.16 ± 0.07	M4	⋯	UKIRT	⋯	1
816	15.4	2014 Aug 24	LP600	3.6	3.50 ± 0.06	120 ± 2	2.66 ± 0.03	M0	⋯	UKIRT	⋯	1
1193	15.0	2014 Aug 26	LP600	3.5	3.08 ± 0.06	7 ± 2	2.81 ± 0.02	M1	⋯	UKIRT	0.01	1
1201	14.9	2012 Aug 04	LP600	2.9	2.81 ± 0.06	236 ± 2	4.26 ± 0.08	M6	K16	UKIRT	⋯	1
1201	14.9	2012 Aug 04	LP600	2.6	3.76 ± 0.06	265 ± 2	5.17 ± 0.12	M7	K16	UKIRT	⋯	1
1441	14.9	2014 Aug 31	LP600	4.0	3.06 ± 0.06	333 ± 2	3.73 ± 0.03	M2	⋯	UKIRT	⋯	1
1804	15.3	2014 Sep 02	LP600	3.2	2.88 ± 0.06	168 ± 2	2.84 ± 0.03	M3	⋯	UKIRT	0.01	1
1995	15.0	2014 Aug 24	LP600	3.1	2.96 ± 0.06	355 ± 2	5.34 ± 0.04	M4	⋯	UKIRT	0.01	1
2050	12.2	2015 Jun 07	LP600	4.6	3.33 ± 0.06	215 ± 2	5.33 ± 0.04	M5	CFOP	⋯	0.01,0.02	2
2206	15.0	2014 Jul 19	LP600	4.6	3.28 ± 0.06	87 ± 2	1.28 ± 0.05	K4	⋯	UKIRT	⋯	1
2379	14.9	2014 Aug 29	LP600	4.8	3.59 ± 0.06	139 ± 2	1.89 ± 0.03	K3	⋯	UKIRT	0.01	1
2579	15.0	2014 Jul 12	LP600	2.7	3.48 ± 0.06	355 ± 2	3.69 ± 0.03	M2	⋯	UKIRT	⋯	3
3066	15.6	2014 Aug 24	LP600	4.3	3.41 ± 0.06	335 ± 2	1.86 ± 0.02	M0	⋯	UKIRT	⋯	1
3111	12.7	2014 Aug 20	i'	3.8	3.36 ± 0.06	234 ± 2	5.87 ± 0.13	M5	D14	⋯	⋯	2
3161	9.6	2015 Jun 03	LP600	2.7	2.68 ± 0.06	67 ± 2	3.04 ± 0.14	K5	CFOP	⋯	0.01	1
3264	15.6	2014 Aug 28	LP600	3.1	3.66 ± 0.06	217 ± 2	1.37 ± 0.02	M0	⋯	UKIRT	⋯	1
3341	14.7	2014 Jul 17	LP600	3.2	3.23 ± 0.06	107 ± 2	4.27 ± 0.08	M3	⋯	UKIRT	⋯	2
3347	15.2	2014 Aug 28	LP600	4.2	3.24 ± 0.06	295 ± 2	2.20 ± 0.02	M0	⋯	UKIRT	⋯	1
3354	14.9	2014 Jul 16	LP600	4.2	3.71 ± 0.06	227 ± 2	2.55 ± 0.06	M0	⋯	UKIRT	⋯	1
3463	14.6	2015 Jun 07	LP600	4.3	3.67 ± 0.06	96 ± 2	4.41 ± 0.04	M3	⋯	UKIRT	⋯	1
3463	14.6	2015 Jun 07	LP600	3.2	2.74 ± 0.06	79 ± 2	4.79 ± 0.02	M4	⋯	⋯	⋯	1
3533	14.4	2014 Nov 09	LP600	4.1	3.08 ± 0.06	10 ± 2	5.21 ± 0.03	M3	⋯	UKIRT	0.01	1
3678	12.6	2014 Jun 17	LP600	2.8	2.63 ± 0.06	170 ± 2	5.08 ± 0.04	M5	W15	UKIRT	⋯	1
4131	13.2	2014 Jun 19	LP600	4.7	2.85 ± 0.06	124 ± 2	5.04 ± 0.02	K7	⋯	UKIRT	0.01	2
4268	14.8	2014 Aug 31	LP600	3.0	3.56 ± 0.06	263 ± 2	4.77 ± 0.04	M6	⋯	UKIRT	⋯	1
4334	15.5	2014 Sep 01	LP600	2.6	3.32 ± 0.06	15 ± 2	3.79 ± 0.06	M4	⋯	UKIRT	⋯	1
4345	13.2	2014 Jul 13	LP600	3.9	3.17 ± 0.06	242 ± 2	3.22 ± 0.02	M2	⋯	UKIRT	0.01	1
4353	15.4	2014 Aug 24	LP600	2.8	3.50 ± 0.06	36 ± 2	2.75 ± 0.04	M0	⋯	UKIRT	0.01	1
4405	14.5	2014 Jul 17	LP600	3.4	2.95 ± 0.06	249 ± 2	3.19 ± 0.02	M0	⋯	UKIRT	0.01	1
4467	15.6	2014 Aug 26	LP600	4.0	3.99 ± 0.06	131 ± 2	4.21 ± 0.04	M4	⋯	UKIRT	⋯	1
4526	15.1	2014 Aug 24	LP600	4.4	2.53 ± 0.06	346 ± 2	4.44 ± 0.02	M3	⋯	UKIRT	⋯	2
4526	15.1	2014 Aug 24	LP600	3.1	3.98 ± 0.06	179 ± 2	4.80 ± 0.09	M4	⋯	UKIRT	⋯	2
4655	15.2	2014 Aug 23	LP600	2.9	3.17 ± 0.06	116 ± 2	3.02 ± 0.05	M0	⋯	UKIRT	⋯	1
4661	14.5	2014 Jul 18	LP600	4.1	3.93 ± 0.06	198 ± 2	2.32 ± 0.05	M2	⋯	J19295122+4117529	⋯	1
4700	15.7	2014 Aug 31	LP600	3.8	3.77 ± 0.06	49 ± 2	1.89 ± 0.05	M0	⋯	UKIRT	⋯	1
4710	15.4	2014 Sep 01	LP600	3.5	2.70 ± 0.06	168 ± 2	3.50 ± 0.05	M2	⋯	UKIRT	⋯	1
4881	12.7	2014 Aug 21	LP600	4.9	3.42 ± 0.06	30 ± 2	3.30 ± 0.03	M0	⋯	UKIRT	0.01,0.02	2
5210	14.9	2014 Jul 14	LP600	3.8	2.71 ± 0.06	267 ± 2	2.22 ± 0.05	M1	⋯	UKIRT	⋯	1
5216	15.3	2014 Aug 31	LP600	3.2	3.67 ± 0.06	96 ± 2	3.31 ± 0.03	M1	⋯	UKIRT	⋯	1

Table 7
(Continued)

KOI	m_i' (mag)	ObsID	Filter	Det. Significance σ	Separation ($''$)	P.A. ($^\circ$)	Mag. Diff. (mag)	Approx. Comp. Spectral Type[c]	Prev. High Res. Detection?	Prev. Low Res. Detection?	False Positive?[a]	$N_{\rm KOI}$[b]
5220	11.8	2014 Sep 03	LP600	3.0	2.83 ± 0.06	109 ± 2	7.22 ± 0.08	M7	⋯	UKIRT	⋯	1
5327	15.0	2014 Sep 01	LP600	3.0	3.63 ± 0.06	277 ± 2	3.92 ± 0.02	M5	⋯	UKIRT	⋯	1
5331	14.9	2014 Aug 31	LP600	3.0	3.67 ± 0.06	351 ± 2	3.72 ± 0.03	M4	⋯	UKIRT	⋯	1
5480	16.3	2014 Aug 29	LP600	3.6	3.52 ± 0.06	174 ± 2	1.24 ± 0.05	K1	⋯	UKIRT	⋯	1
5556	13.2	2014 Jun 13	LP600	3.6	3.28 ± 0.06	162 ± 2	4.31 ± 0.03	M4	CFOP		⋯	1
5556	13.2	2014 Jun 13	LP600	3.4	3.22 ± 0.06	247 ± 2	5.29 ± 0.02	M5	CFOP	⋯	⋯	1
5707	15.0	2014 Aug 23	LP600	3.3	2.71 ± 0.06	239 ± 2	2.43 ± 0.02	K7	⋯	UKIRT	⋯	1
5885	14.7	2014 Aug 21	LP600	2.8	3.42 ± 0.06	127 ± 2	4.03 ± 0.04	M3	⋯	UKIRT	⋯	1
6120	15.4	2015 Jun 08	LP600	3.3	3.85 ± 0.06	128 ± 2	2.48 ± 0.02	M0	⋯	J19214830+3951405	⋯	2
6560	12.9	2015 Jun 06	LP600	4.8	3.28 ± 0.06	246 ± 2	6.04 ± 0.12	M6	⋯	UKIRT	0.01	1
6605	11.3	2015 Jun 08	LP600	4.2	2.53 ± 0.06	320 ± 2	3.46 ± 0.04	M0	CFOP	⋯	⋯	1
6610	15.3	2015 Jun 12	LP600	3.5	2.63 ± 0.06	216 ± 2	1.22 ± 0.02	G3	⋯	UKIRT	⋯	1
6745	15.2	2015 Jun 12	LP600	2.7	3.07 ± 0.06	72 ± 2	3.78 ± 0.02	M0	⋯	UKIRT	⋯	1
6745	15.2	2015 Jun 12	LP600	2.5	2.85 ± 0.06	163 ± 2	3.92 ± 0.03	M0	⋯	UKIRT	⋯	1
6800	12.8	2015 Jun 12	LP600	2.7	2.62 ± 0.06	145 ± 2	5.10 ± 0.04	M4	⋯	UKIRT	0.01	1
6800	12.8	2015 Jun 12	LP600	2.9	3.11 ± 0.06	337 ± 2	5.41 ± 0.04	M5	⋯	UKIRT	0.01	1
6925	15.7	2015 Jun 03	LP600	3.1	2.66 ± 0.06	125 ± 2	1.71 ± 0.12	M4	⋯	UKIRT	⋯	1

Notes. References for previous detections are denoted using the following codes: Lillo-Box et al. 2012 (LB12), Dressing et al. 2014 (D14), Kraus et al. 2016 (K16), visible in United Kingdom InfraRed Telescope images (UKIRT), companions visible in UKIRT and with 2MASS designations (J*).

[a] Probability that planetary transit signal is a false positive based on *Kepler* data.

[b] Number of planet candidates detected orbiting KOI.

[c] Estimation method described in Section 3.7.3.

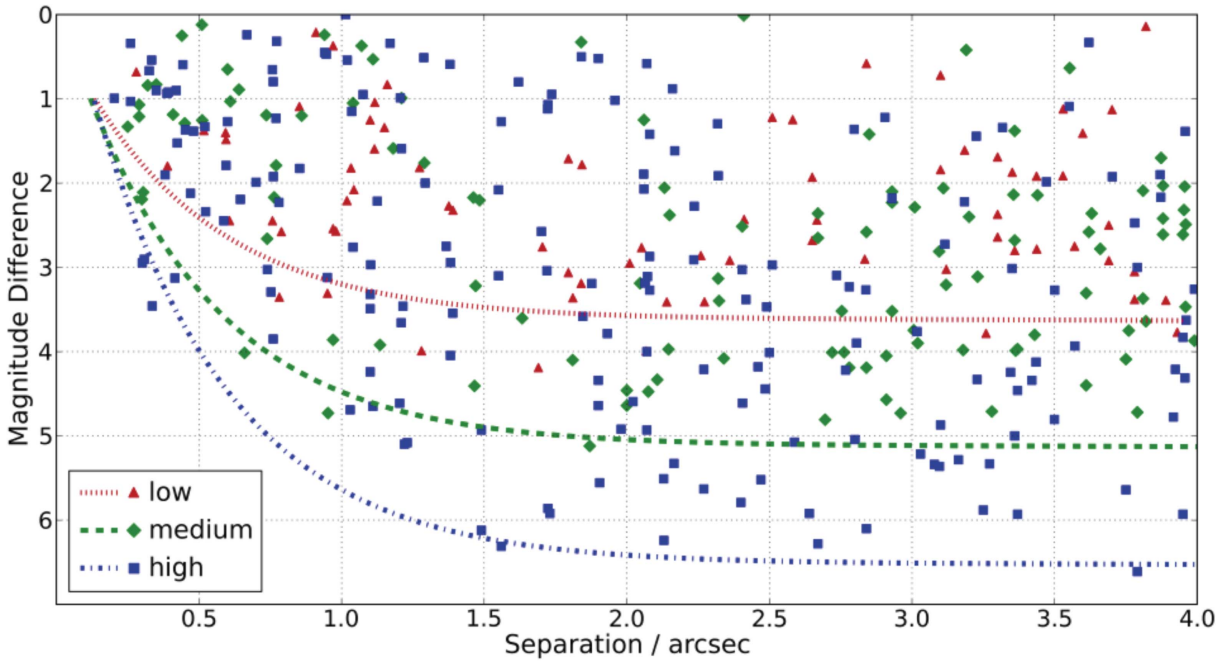

Figure 5. Separations and magnitude differences of the detected companions in Paper II and this work, with the color and shape of each star denoting the associated typical low-, medium- and high-performance 5σ contrast curve during the observation (as described in Section 3.6).

3.7.2. Separation and Position Angles

Separation and position angles were determined from the raw pixel positions. Uncertainties were found using estimated systematic errors due to blending between components. Typical uncertainty in the position for each star was 1–2 pixels. Position angles and the plate scale were calculated using a distortion solution produced using Robo-AO measurements for the globular cluster M15.[9]

3.7.3. Companion Spectral Types

The approximate spectral type of the detected companions, assuming that they are bound to the primary and all stars are main sequence dwarfs, were estimated using a spectral energy distribution model (Kraus & Hillenbrand 2007) and the estimated stellar effective temperatures reported on the NASA Exoplanet Archive. With the LP600 band closely matching the *Kepler* bandpass, the magnitude differences between the primary star and nearby stars were converted to i'-band when necessary using the linear correlation found by Lillo-Box et al. (2014):

$$\Delta m_{i'} = 0.947 \cdot \Delta m_{LP600}. \quad (1)$$

In addition, we estimate the latest spectral type companion consistent with a 5σ detection for each observed target based on the typical contrast curve for the three image performance groups (see Section 3.6). These estimates are listed in Table 9 in the Appendix.

We caution that these spectral types are approximate and do not account for factors such as giant contamination, estimated at ~12% by Ciardi et al. (2011). In addition, the use of a linear correlation in converting between passbands will result in an error with varying spectral types. We estimate this error by calculating the flux of F0V to M5V stars (Pickles 1998) in the LP600 and i'-band, including quantum efficiencies and instrumental effects (see Figure 2 in Paper I). The maximum difference between the flux of spectral types in the two passbands results in an error of ~0.15 mag, equivalent to approximately one subspectral type.

4. DISCOVERIES

Of the 1629 KOI targets observed, 206 are apparent in multiple star systems for a nearby star fraction within 4″ of 12.6% ± 0.9%.[10] We also found 15 triple systems for a triplet fraction of $0.92^{+0.30}_{-0.18}$%,[11] and 1 quadruple system for a quadruplet fraction of $0.06^{+0.14}_{-0.02}$% (see footnote 11). Cutouts of the triple and quadruple systems are shown in Figure 6. One quarter (25.8%) of the companions would only be observable in a high-resolution survey (<1.″0 separation), and one half (49.8%) of the companions are too close (<2.″0) for many seeing limited surveys to accurately measure binary properties (e.g., contrast ratios). The detected companion separations and contrast ratios are plotted in Figure 5, along with the calculated 5σ detection limits, as detailed in Section 3.6. Cutouts of all multiple star systems are shown in Figures 18–21. For companions within 2.″5, measured properties are detailed in Tables 4 and 6. For companions outside 2.″5 but within 4.″0, measured properties are detailed in Tables 5 and 7.

We confirmed six companions to eight Robo-AO detections with NIRC2 and AO on Keck II (Wizinowich et al. 2000). In addition, two new companions were found around KOIs 2554 and 3020. These targets were selected for followup because of their faintness and/or closely separated detected companion. Low-sigma, visually detected companions to KOIs 1873 and 5257 were not detected. These non-detected companions are possibly a result of non-common path aberrations, as described in Section 5.1 of Paper II. These spurious detections all have

[9] S. Hildebrandt (2013, private communication).

[10] Error based on Poissonian statistics (Burgasser et al. 2003).

[11] Error based on binomial statistics (Burgasser et al. 2003).

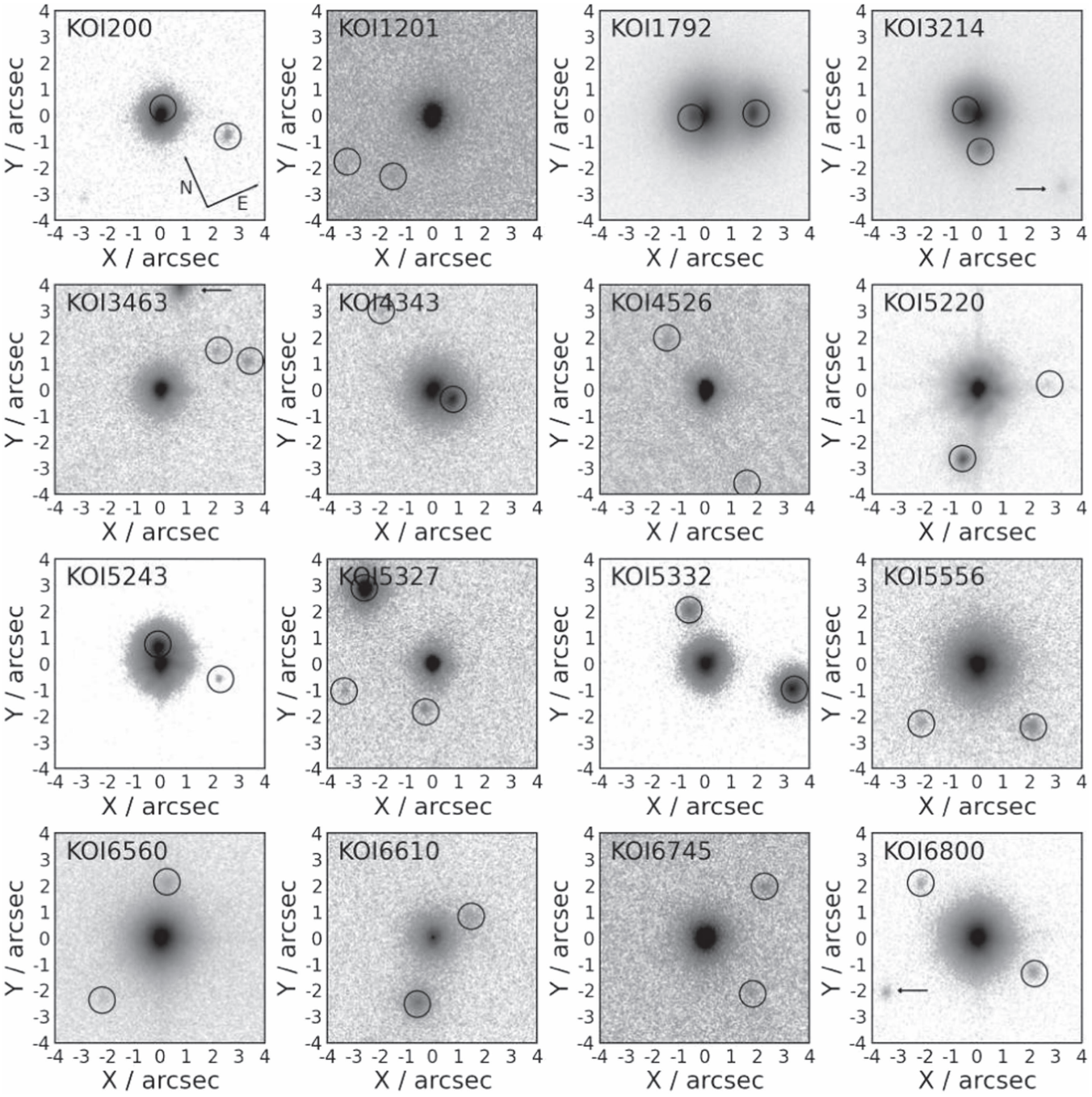

Figure 6. Normalized log-scale cutouts of 16 KOIs with multiple companions with separations $<4''$ resolved with Robo-AO. The angular scale and orientation (displayed in the first frame) is similar for each cutout, and circles are centered on the detected nearby stars. Three targets (KOIs 3214, 3463, and 6800) have a possible third companion, marked with arrows, outside our $4''$ separation cutoff, as described in Section 5.2.1.

similar separations and position angles with respect to the target star, facilitating their identification and manual removal. The PSF subtraction routine usually does not remove these false companions, as another star exhibiting the NCP error is unlikely to be within the set of twenty reference images. The Keck II observations are listed in Table 2, with the measured separations and position angles of the confirmed companions using Keck II images listed in Tables 4 and 6, and the follow-up images are shown in Figure 7.

We confirmed five companions to seven KOIs observed in this paper with NIRI and AO on Gemini North. We did not detect a possible companion to KOI-2198 that was visually detected, manifesting as an elongated PSF in the Robo-AO image. We observed three KOIs targeted in Paper I (KOI-327) and Paper II (KOIs 2833 and 4301), which displayed non-common path error aberrations. No companions were observed to these three targets in the follow-up observations. A new companion outside our separation cutoff ($\rho = 4\farcs24$) was observed near KOI-4131. The Gemini observations are listed in Table 3, and the follow-up images are shown in Figure 8.

4.1. Comparison to Other Surveys

Two detected companions (KOI-326 and KOI-841) in our survey were previously found in Lillo-Box et al. (2012), who

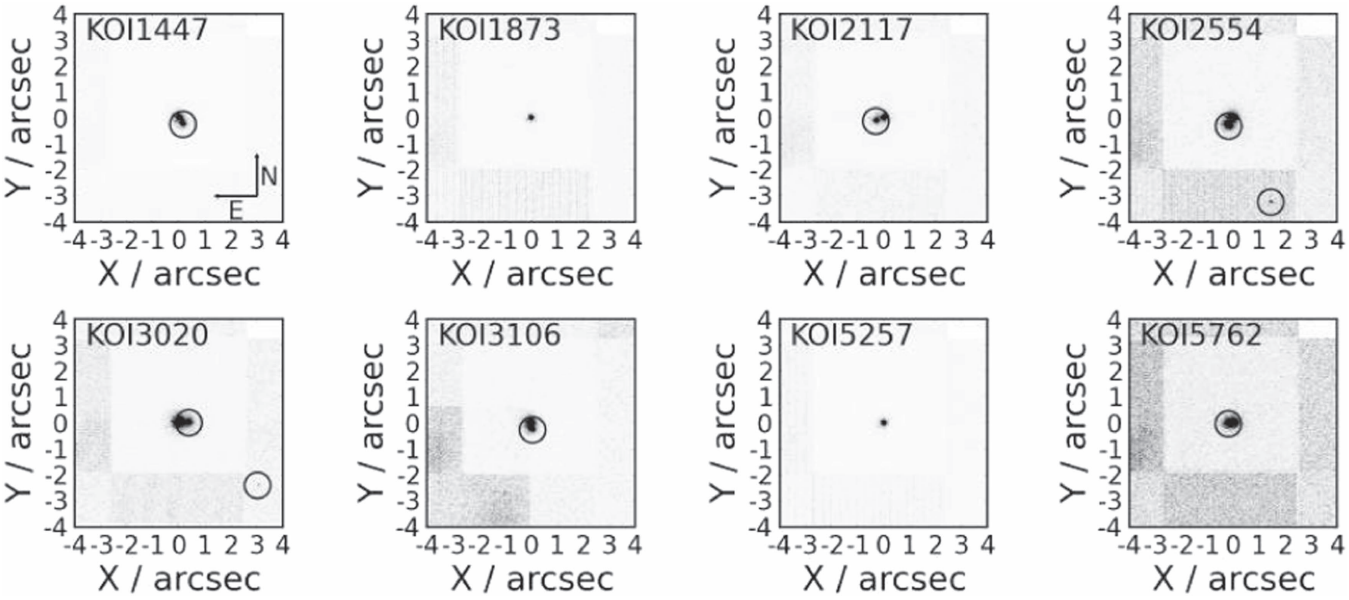

Figure 7. Normalized log-scale cutouts of 8 KOIs observed with the NIRC2 instrument on Keck II, as described in Section 2.2.2. The angular scale and orientation (displayed in the first frame) is similar for each cutout, and circles are centered on the detected nearby stars.

observed 98 KOIs using the AstraLux Lucky Imaging system on the 2.2 m telescope at the Calar Alto Observatory. Lillo-Box et al. (2014) also previously detected companions to KOI-3263, 3649, and 3886 in a survey of 174 KOIs. Adams et al. (2012, 2013) observed 87 and 13 KOIs, respectively, with the instruments ARIES and PHARO on the MMT and Palomar telescopes, respectively. They detect companions to KOI-126 and 266 that are fainter than our survey sensitivity. Observing 87 KOIs with ARIES at the MMT, Dressing et al. (2014) previously detected companions to KOI-2813 and KOI-3111 and also detected a companion to KOI-266 ($\Delta m_{K_s} = 6.32$) that is outside our detection sensitivity. Gilliland et al. (2015) found two companions to KOI-829 using the *Hubble Space Telescope* (*HST*) with Δm_{K_p} of 2.4 and 6.0 and separations of 0.″11 and 3.″31, respectively, which were outside the detection limits of our Robo-AO image. Wang et al. (2015a) observed 84 KOIs using the PHARO and NIRC2 instruments at Palomar and Keck, respectively, with one discovered companion (KOI-3678) appearing in our survey. Two of our targets (KOI-1411 and KOI-3823) have companions detected by Wang et al., both with $\Delta m_K > 5$, which fall outside our detection sensitivity. Wang et al. (2015b) observed 73 multiple transiting planet KOI systems at Palomar and Keck, with the only overlapping system being a companion observed near KOI-1806 that we did not detect. The companion to KOI-1806, measured by Wang et al. (2015b) as $\Delta K = 1.45$ at 3.″43 separation, is well within our survey sensitivity, and the reason for the non-detection is unclear. The reported companion is also not visible in UKIRT images, although it would be detectable. We detected companions to KOI-126 and -200, not detected by Howell et al. (2011); both companions are within the stated sensitivity limits for their respective targets, so the reason for the earlier non-detection is unclear. None of our nearby-star detections overlap with the discoveries of Everett et al. (2015).

Kraus et al. (2016) observed 382 KOIs with AO on the Keck II telescope. They detected single companions to KOI-255, 1908, 2705, and 2813, and both companions to KOI-1201 that were detected in our survey. They also detected single companions to KOI-1298, 1681, 2179 2453, and 2862, and double companions to KOI-1361 and 2813, that all fall outside of our reported sensitivity.

Kolbl et al. (2015) searched for the blended spectra of KOIs with secondary stars within ∼0.″8 using Keck-HIRES optical echelle spectra of 1160 California *Kepler* Survey KOIs. Of the 63 KOIs the authors found with evidence of a secondary star, we found companions to seven (KOIs 1137, 2813, 3161, 3415, 3471, 4345, 4713) and did not detect companions to eight (KOIs 1121, 1326, 1645, 3515, 3527, 3605, 3606, 3853). The companions we did not detect likely lie at small separations inside the limits of our survey sensitivity. Two of our companions (KOIs 1137 and 3415) fall within their calculated flux ratio uncertainty and their ∼0.″8 separation limit. Without known separations and position angles, however, it is not clear that these are the same companion stars.

Nine of the widest nearby stars we detected have 2MASS (Skrutskie et al. 2006) designations. 102 of our wide ($\rho > 2''$) nearby star detections are noted on the *Kepler* Community Follow-up Observing Program using J-band, ∼1″ seeing-limited imaging from United Kingdom InfraRed Telescope (UKIRT) (Lawrence et al. 2007). However, with high-acuity imaging to resolve blended companions, providing greater precision photometry, and a filter that better simulates the *Kepler* bandpass, the Robo-AO survey can better evaluate the effect of the companion on the observed transit signal.

4.2. Multiplicity and Other Surveys

There have been multiple past high-resolution surveys of KOIs performed, allowing our results to be put into context with the overall community follow-up program. A comparison of the observed nearby-star rates from various surveys with differing methodologies may also provide convergence on the intrinsic multiplicity rate of planet hosting stars. With varying sensitivities between surveys, we use a lower separation cutoff than in this paper for a uniform comparison between surveys. This also has the added benefit of using only the nearest stars that have the highest probability of association. An exact comparison between surveys is still hindered, however, by the

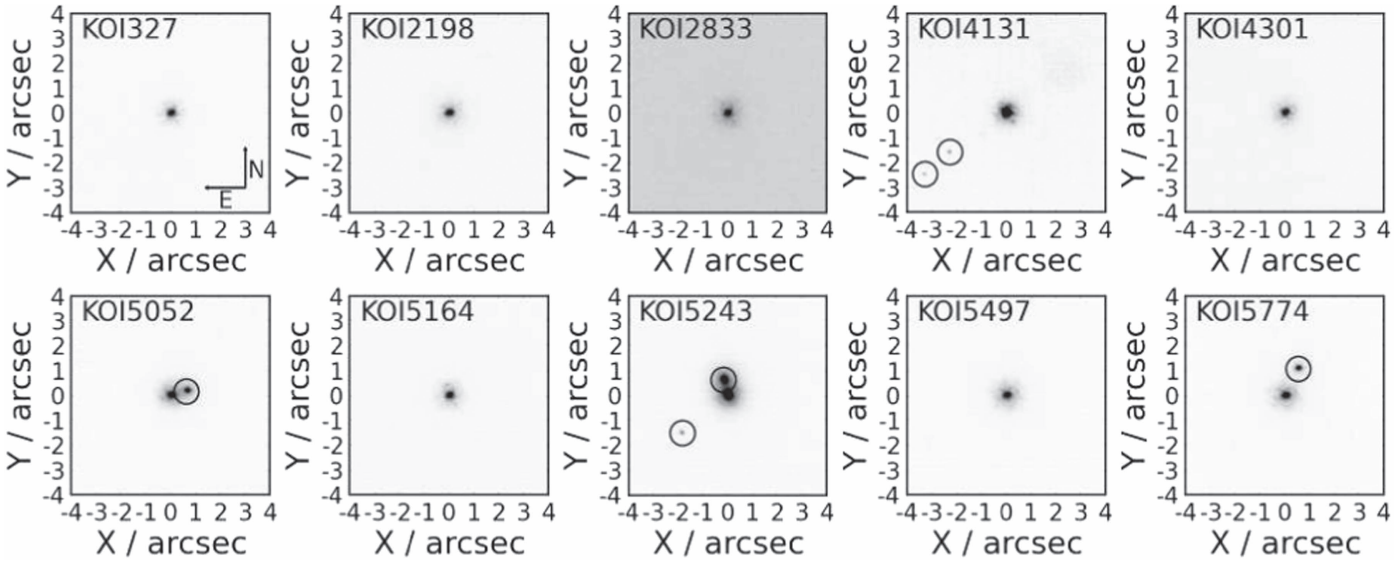

Figure 8. Normalized log-scale cutouts of 10 KOIs observed with the NIRI instrument on Gemini North, as described in Section 2.2.3. The angular scale and orientation (displayed in the first frame) is similar for each cutout, and circles are centered on the detected nearby stars.

use of dissimilar instruments, passbands, and target selection criteria; in comparing results in this section, we attempt to highlight major differences when comparing multiplicity rates. However, we caution that in each case there are inherent biases in the coverage of the different surveys that require detailed analysis not covered in this work.

We find that 6.8% of KOIs have nearby stars within 2″, in agreement with other visible light surveys: 6.4% in Paper I, 8.2% in Paper II, and 6.4% (Howell et al. 2011). Horch et al. (2014) found 7.0% of KOI targets had nearby stars within 1″ separation, a range where we showed a 3.4% nearby star rate. Horch et al. (2014) do not report their target list, so it is not possible to identify the source of this discrepancy. It is possible that this is a result of our target selection of every KOI, resulting in a dimmer overall sample than surveys which prioritize brighter targets. The targets in this paper have a median $K_{p,\mathrm{med}} = 14.9$, significantly fainter overall than the targets in Adams et al. (2012, $K_{p,\mathrm{med}} = 12.2$), Dressing et al. (2014, $K_{p,\mathrm{med}} = 13.3$) Wang et al. (2015a, $K_p < 14$) Paper I ($K_{p,\mathrm{med}} = 13.7$), and in Paper II ($K_{p,\mathrm{med}=14.2}$). Horch et al. (2014) note that their *Kepler* targets are mainly between 11th and 14th magnitude. There are several reasons a brighter overall target list will inflate binarity rates: the target stars are intrinsically more luminous, which results in more physically associated companion stars as binarity correlates with luminosity (Duchêne & Kraus 2013); the target stars are less distant, so the physically associated companion of a given spectral type is brighter, and thus easier to detect. Brighter stars also tend to have deeper detectable contrast ratios.

The disparity in multiplicity between papers in the Robo-AO survey was explored in Section 6 of Paper II as a possible result of the bias in the KOI selection process between data releases, with the median observed KOI in Paper II located nearer the Galactic plane than in Paper I. KOIs near the Galactic plane lie in denser stellar fields, increasing the likelihood of unassociated nearby stars with the separation cutoff. Plotting the *Kepler* field of view with our targeted KOIs in Figure 3, the median position of KOIs in this work is closer to the center of the field than in Paper II, and further from the Galactic plane than Paper I or Paper II.

Surveys in the NIR find higher multiplicity rates within 2″: 13% (Dressing et al. 2014), 17% (Adams et al. 2012), 20% (Adams et al. 2013). This is likely caused by many companions being cool, red dwarf stars that are faint in the optical (Ngo et al. 2015), and deeper, higher angular resolution imaging.

5. DISCUSSION

In this section, we delve further into the combined data sets of Paper II and this work to explore the implications of stellar multiplicity on the planetary candidates (Section 5.1), expand on the planetary candidates found in higher order multiple systems or orbiting within the habitable zone (HZ) (Section 5.2), and search for insight into the role that multiple stellar bodies play on planetary formation and evolution (Section 5.3).

5.1. *Implications for* Kepler *Planet Candidates*

When a close companion is detected near a KOI host star, there are several potential implications. If the planet does indeed transit the purported target star, the consequences may be relatively mild; the planet's radius will be slightly larger than had previously been thought—at most by a factor of $\sqrt{2}$ in the case of an equal-brightness companion (Ciardi et al. 2015). If the eclipsed star is a faint companion, however, the radius of the eclipsing object may be many times larger, potentially turning a small planet into a giant planet or a planet into a false-positive eclipsing binary star. Additionally, as the properties of most of the host stars in the *Kepler* stellar catalog are based on broad-band photometry assuming that they are single, the derived stellar radii may well be incorrect if the system actually contains multiple stars. Re-fitting the stellar properties of all the companion stars—as well as for the *Kepler* target stars accounting for the presence of the companions—is beyond the scope of this work, but will be addressed in a future paper in this series.

Finally, if a KOI system has multiple transiting planets detected, it might be the case that the planets are distributed around multiple stars in the system. KOI-284/Kepler-132 is a good example of such a case (Fabrycky et al. 2012; Lissauer

et al. 2014); its multiple planets would be unstable if they all orbited a single star, but it turns out to be a close visual binary, with the only sensible interpretation being that some of the planets transit one star and some transit the other. Although such "split multiple" systems are predicted to be relatively rare among the population of *Kepler* multiple stellar systems (Fabrycky et al. 2012), any multi-planet system with a close companion has a higher chance of being split, and thus deserves close consideration. Barclay et al. (2015) present a model of how such systems might be analyzed, investigating the KOI-1422/Kepler-296.

5.2. Particularly Interesting Systems

Several KOIs with detected companions are of particular interest for displaying unusual system characteristics, rare false-positive scenarios, or planetary attributes that satisfy habitability requirements.

5.2.1. Possible Quadruple Systems

KOI-5327 hosts a 2.24 $R_\oplus$ planetary candidate on a 5.4 day orbit. We detect two nearby stellar companions, with angular separations of 1.″88 and 3.″63 and magnitude differences of 3.43 and 3.92, respectively. A possible fourth component of the system lies at 3.″96, and is 0.12 mag brighter than the KOI target. Further multiple passband observations and radial velocity measurements are needed to understand the hierarchy of this system. In the full 44″ square image, a total of eight stars appear, including the target and possible companions. With nearly equal brightness, the third companion has a high probability of being associated. With few stars found in the full field, it is unlikely that any unassociated stars would be found within 4″ of the KOI. The likelihood that the other two stars are, in fact, bound is 97%. If physical association is confirmed for all four components, KOI-5327 would be the third known planet residing in a quadruple star system (Schwamb et al. 2013; Roberts et al. 2015). Following the analysis of Section 5.1 in Paper I, with the planet assumed to orbit the bright target star, the updated planetary radius estimate for the planetary candidate with all three stars in the aperture is 3.3 $R_\oplus$. Without the 0.12 mag brighter star in the photometric aperture, the updated radius estimate is 2.3 $R_\oplus$. The second scenario detailed in Paper I, with the planet orbiting one of the fainter companions, will be further explored in future papers regarding this survey for all detected companions.

KOI-4495, first detected in Paper II, has three nearby stars, with angular separations of 3.″04, 3.″06, and 3.″41 and magnitude differences of 4.73, 3.90, and 2.68, respectively. The system hosts a planetary candidate with period of 5.92 days and estimated radius of 1.49 $R_\oplus$. The system lies in a relatively dense stellar field; thus, it is probable that at least one of the stars is an unassociated asterism. The Robo-AO discovery image is available in Figure 5 of Paper II. With all three stars in the photometric aperture diluting the transit signal, and assuming the planet does indeed orbit the bright star, the updated planetary radius estimate is 1.6 $R_\oplus$.

KOI-3214 hosts planetary candidates with radii of 2.59 $R_\oplus$ and 2.02 $R_\oplus$ on 11.5 and 25.1 day orbits, respectively. We detect two nearby stellar companions, with angular separations of 0.″49 and 1.″41 and magnitude differences of 0.73 and 2.50, respectively. Outside our 4″ separation cutoff, another 5.33 mag dimmer star appears at and 4.″34. With multiple stars in the same *Kepler* pixel, the probability of an eclipsing binary resulting in a false planetary transit signal is increased. KOI-3214 lies in a relatively sparse stellar field, with only six additional stars in the full 44″ square image, including the target and possible companions. The probability based on the background star density that all three stars are bound is approximately 98%. Assuming the planets orbit the brightest star, the two close stars likely dilute the observed transit signal, leading to updated planetary radii estimates of 3.3 $R_\oplus$ and 2.6 $R_\oplus$ for the planet candidates on orbits with periods of 11.5 and 25.1 days, respectively.

KOI-3463 hosts a 1.3 $R_\oplus$ planetary candidate on a 32.5 day orbit. We detect two nearby stellar companions, with angular separations of 2.″74 and 3.″67 and magnitude differences of 4.79 and 4.41, respectively. Just outside our 4″ separation cutoff, another 2.44 mag dimmer star appears at 4.″11. KOI-3463 lies in a relatively dense stellar field, with at least 16 stars in the full 44″ square image, including the target and possible companions. The probability, based on the background star density, that all three stars are bound is approximately 86%. If the planet candidate orbits the bright star, the additional two nearby stars in the photometric aperture only marginally dilute the transit signal, leading to an updated planetary radius estimate of 1.3 $R_\oplus$.

KOI-6800 hosts a 27.5 $R_\oplus$ planetary candidate on a 2.5 day orbit. We detect two nearby stellar companions, with angular separations of 2.″62 and 3.″11 and magnitude differences of 5.10 and 5.41, respectively. Outside our 4″ separation cutoff, another 5.27 mag dimmer object appears at 4.″13, although UKIRT photometry suggests that this is highly likely (>99%) a background galaxy. In the full 44″ square image of KOI-6800, nine stars are visible, including the target and possible companions. The probability, based on the background star density, that all three stars are bound is approximately 97%. The two dim nearby stars within the photometric aperture only slightly increases the estimated planetary radius to 27.7 $R_\oplus$, assuming the planet orbits the brightest star. If the planet candidate orbits one of the fainter stars, the corrected planetary radius would be large enough to make it highly probable the transiting event is in fact a background eclipsing binary.

The Robo-AO images of the four possible quadruple systems from this work are displayed in Figure 6.

5.2.2. HZ Candidates

The discovery of habitable exoplanets is a major goal of the *Kepler* mission, and an accurate knowledge of the host star's properties is required to establish unambiguously whether an exoplanet possesses the two habitability conditions—rocky and in a location where water can be found in a liquid state on the surface HZ. The exact requirements for habitability are still debated (Kasting et al. 1993; Selsis et al. 2007; Seager 2013; Zsom et al. 2013); however, it has been shown that the transition between "rocky" and "non-rocky" occurs rather sharply at $R_P = 1.6R_\oplus$ (Rogers 2015). For this analysis, we will use a large cutoff of 4 $R_\oplus$, as the presence of a stellar companion may dramatically alter the estimated radius, and even a gaseous planet in the HZ may host a rocky exomoon (Heller 2012). Overall, the existence of an unknown stellar companion within the same photometric aperture as the KOI will increase the calculated radius of the planet, as the observed transit signal will be diluted by the constant light of the nearby star.

Table 8
Habitable Zone Candidates with Robo-AO Detected Companions

Planet Candidate	Period (day)	$R_{p,i}$[a] ($R_\oplus$)	$R_{p,c}$[b] ($R_\oplus$)	Equil. Temp. (K)	Sep ($''$)	Δm (mag)
227.01[c]	17.7	2.45	2.96	350	0.33	0.84
255.01	27.5	2.51	2.67	313	3.36	2.14
438.02[c]	52.7	1.76	1.81	271	3.28	3.11
1503.01	150.2	3.79	4.23	291	0.76	1.52
1846.01	106.0	3.81	4.46	322	3.7	1.07
1989.01[c]	201.1	1.84	1.88	297	1.12	3.49
2174.02[c]	33.1	1.88	2.53	343	0.92	0.21
2744.01	109.6	2.46	2.63	340	3.44	2.12
2760.01	56.6	2.19	2.64	317	0.44	0.84
2862.01	24.6	1.79	2.44	321	0.67	0.17
2926.03	21.0	2.43	3.24	357	0.33	0.27
2926.04	37.6	2.09	2.79	294	0.33	0.27
3255.01[c]	66.7	1.37	1.38	294	3.15	4.87
3284.01[c]	35.2	0.98	1.03	272	3.94	2.42
3401.02[c]	326.7	2.20	2.64	283	0.65	0.89
3946.01[c]	308.5	2.36	2.37	298	4.27	5.26
4550.01	140.3	1.73	2.42	257	1.03	0.04
4810.01	115.2	2.07	2.13	353	2.32	3.16
5101.01	436.2	1.64	1.68	331	1.22	3.33
5553.01	120.9	2.59	2.71	333	0.95	2.52
5671.01	190.9	1.73	1.89	356	2.13	1.79
5707.01	208.8	2.8	3.03	347	2.67	2.43
5885.01	111.1	1.87	1.89	364	3.36	4.03
6120.02	205.4	1.67	1.75	323	3.78	2.48
6745.01	383.9	2.78	2.82	314	3.02	3.78
6745.01	383.9	2.78	2.82	314	2.81	3.92

Notes.
[a] Initial planetary radius estimate.
[b] Corrected planetary radius estimate.
[c] Detected in Paper II of this survey.

In Paper II and this work, we detected companions to 26 KOIs that host planetary candidates with equilibrium temperatures, from the NEA, in the HZ range (273 K $\leqslant T_{\rm eq} \leqslant$ 373 K) and $R < 4\ R_\oplus$, displayed in Table 8. All are newly detected in this survey. Corrected planetary radii estimates are included, as described in Section 5.1 of Paper I, with the assumption that the planet orbits the bright star.

KOI-2926 hosts two planetary candidates within the HZ, and KOI-6745 is a possible triple system hosting a planet in the HZ. The equilibrium temperature calculation is based on an estimate of the stellar effective temperature of the host star. Thus, if the planet orbits the dimmer companion, it is unlikely to be in the HZ.

KOI-1503 hosts a planetary candidate with initial diluted radius estimate of 3.79 $R_\oplus$ in a 0.51 AU orbit. If the planet orbits the primary star, the corrected radius of the planet is 4.23 $\pm$0.07 $R_\oplus$, decreasing the probability that it is rocky.

KOI-5101, a Sun-like star, hosts a near-Earth analog, with a calculated radius 64% larger than Earth and an orbit of 1.12 AU. With a 3.33 mag dimmer companion at 1.″22, the KOI is likely a 1.68 $R_\oplus$ rocky planet if it orbits the primary.

5.3. Stellar Multiplicity and Kepler Planet Candidates

We detect 206 planetary candidate hosts with nearby stars from 1629 targets, for an overall multiplicity fraction of 12.6% $\pm$ 0.9% within the detectability range of our survey (~0.″15–4.″0, $\Delta m \leqslant 6$). For this analysis, we will combine the results in this work with those from Paper II. With this large data set, we continue the search that began in Paper I for broad-scale correlations between the observed stellar multiplicity and planetary candidate properties. Such correlations provide an avenue to constrain and test planet formation and evolution models.

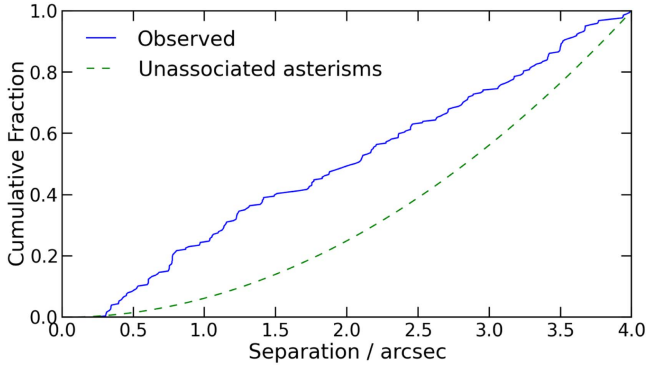

Figure 9. Cumulative distribution of nearby stars within a given separation from our observations in Paper II and this work, and the expected distribution from a set of the same number of unassociated stars. For all separations, the observed number of companions we detected is above the expected number if all stars were unassociated.

Any individual companion found may not be physically bound; however, we expect a small number of unassociated asterisms within our complete set of observed targets. An argument for the majority of nearby stars being associated is derived from the observed distribution of companion separations: if all companions were unassociated background or foreground stars, we would expect a quadratic distribution of companions (i.e., ~4× the number of objects at 4″ as at 2″). Instead, we find a near linear distribution. The dissimilarity between the observed distribution and the distribution of all unassociated objects is shown in Figure 9. In addition, a recent follow-up study with the NIRC2 instrument on the Keck II telescope (Atkinson et al. 2016) observed 84 KOI systems, finding that at least $14.5^{+3.8}_{-3.4}$% of companions within ~4″ are inconsistent with being physically associated based on multi-band photometric parallax. We therefore expect the overall multiplicity trends to remain relatively unchanged when the unassociated objects are removed.

A summary and analysis paper in the Robo-AO survey will investigate the multiplicity properties of *Kepler* candidates in more detail, including quantifying the effects of association probability and incompleteness.

All stellar and planetary properties for the KOIs in this section were obtained from the cumulative planet candidate list at the NASA Exoplanet Archive,[12] and have not been corrected for possible dilution due to the presence of nearby stars.

5.3.1. Stellar Multiplicity and KOI Number

The early and late public releases of KOIs (Borucki et al. 2011b; Batalha et al. 2013; Burke et al. 2014; Thompson et al. 2015) could conceivably have a built-in bias, either astrophysical in origin or as a result of the initial vetting process by the *Kepler* team. This bias might appear as a variation in multiplicity with respect to KOI number. With a target list of KOIs in Paper II and this work widely dispersed in the full KOI data set, we can search for such a trend. The fraction of KOIs

[12] http://exoplanetarchive.ipac.caltech.edu/

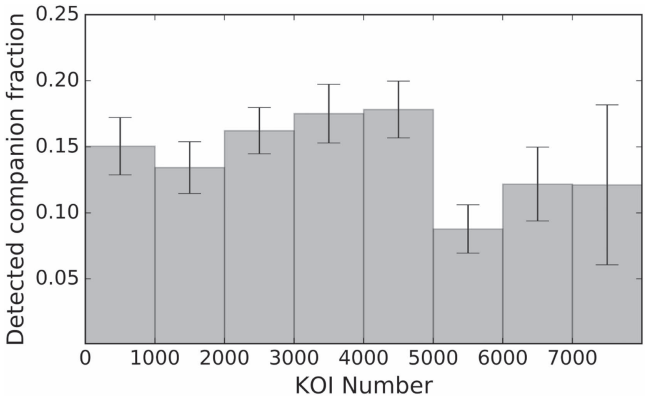

Figure 10. Multiplicity fraction within 4″ of KOIs as a function of KOI number. A 2.9σ decrease in the fraction of nearby stars between KOIs numbered less than 5000 and greater than 5000 is apparent.

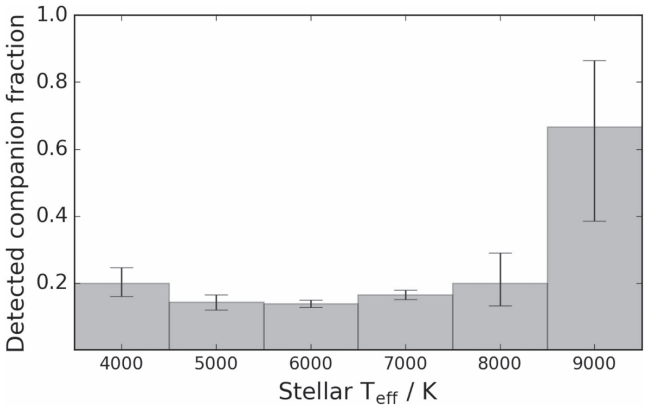

Figure 11. Fraction of KOIs with detected nearby ($\leqslant$4″) stars as a function of stellar effective temperature.

with companions as a function of KOI number, as displayed in Figure 10, shows a sharp decrease at approximately KOI-5000. We find KOI numbers less than 5000 have a nearby star fraction of 16.1% ± 0.9%, and KOI numbers greater than 5000 have a nearby star fraction of 10.2% ± 1.5%, a 2.9σ disparity. The exact mechanism for this is unclear; however, this may be a result of better false positive detection in the later data releases due to automation of the vetting process (Mullally et al. 2015). There is no significant corresponding variation in the separations or contrasts of stellar companions between the two populations.

5.3.2. Stellar Multiplicity Rates and Host-star Temperature Revisited

It has been well-established that stellar multiplicity correlates with stellar mass and temperature (Duchêne & Kraus 2013). In Paper I, it was found (at low significance) that this trend appears to also be true for the observed KOIs. Ngo et al. (2015) found in a sample of stars hosting close-in giant planets that, with 2.9σ significance, stars hotter than 6200 K have a companion rate two times larger than their cool counterparts. We find in the combined target sample of Paper II and this work that 14.7% ± 0.9% of KOIs below 6200 K have a companion, compared to 17.2% ± 2.0% above 6200 K. A Fisher exact test gives an 83% probability that the two samples are indeed from two distinct populations. The trend toward higher multiplicity with higher stellar temperatures is still visually evident, as seen in Figure 11. With an emphasis on solar analogs in the input catalog, the majority of KOIs are FGK-type stars (Batalha et al. 2013); thus, the small number of early-type stars in our sample prevents any high-significance conclusions.

5.3.3. Stellar Multiplicity and Multiple-planet Systems Revisited

Multiple star systems are thought to more commonly host single transiting planets than multiple planet systems. Perturbations from the companion star will change the mutual inclinations of planets in the same system (Wang et al. 2014); therefore, a lower number of multiple transiting planet systems are expected to have stellar companions. Multiple planet systems are also subject to planet-planet effects (Rasio & Ford 1996; Wang et al. 2015a).

In Paper I, we found a low-sigma disparity in multiplicity rates between single- and multiple-planet systems, with single-planet systems exhibiting a slightly higher nearby star fraction. With our combined sample from Paper II and this work, we revisit this result with over three times more targets. We find a slightly higher nearby star fraction for multiple planetary systems, displayed in Figure 12. A Fisher exact test gives an 8.7% probability of this being a chance difference. With the expectation—given the effects of stellar perturbations and the higher false positive rate for single star systems—of a higher nearby-star fraction for single-planet candidate hosting stars, even this low-significance result is surprising. A possible explanation is that the additional stellar body in the system is causing orbital migration of outer planets, moving them to shorter period orbits where *Kepler* has higher sensitivity to transit events. Also, multiple star systems have at least twice as many stars that could host transiting planets, resulting in a higher probability of observing multiple planetary transits. Lastly, with relatively low-significance, this result could also be a consequence of the "look-elsewhere" effect inherent to any multi-comparison study (Gross & Vitells 2010); with the parameter space explored in this section, a result of this significance is expected to arise approximately 50% of the time out of per chance.

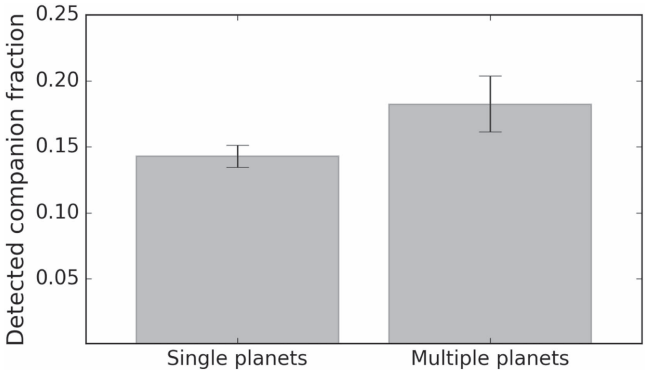

Figure 12. Multiplicity fraction within 4″ of KOIs hosting detected single- and multiple-planetary systems.

Wang et al. (2015b) studied the influence of stellar companions on multiple-planet systems, finding a 3.2σ deficit in multiplicity rate in multi-planet systems, compared to a control sample of field stars. However, they also found no significant disparity in multiplicity rates between single- and multi-planet systems.

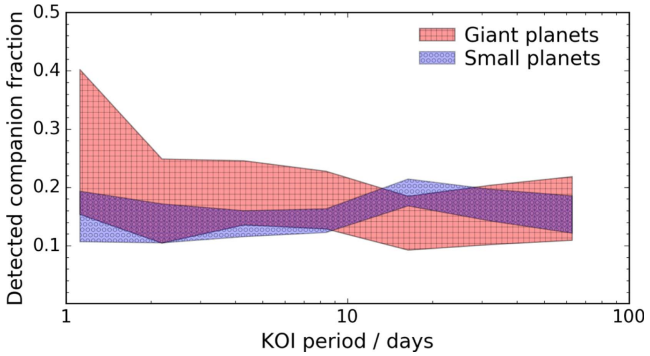

Figure 13. 1σ uncertainty regions for the binarity fraction as a function of KOI period for two different planetary populations.

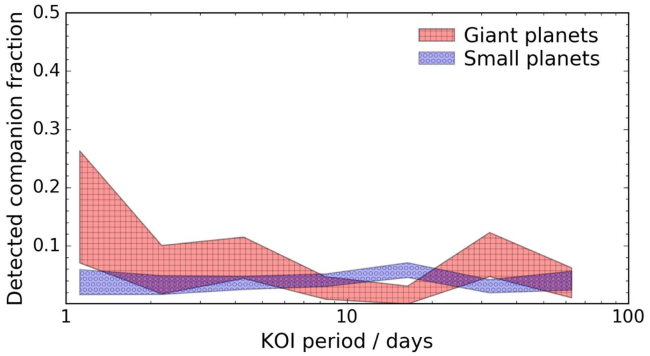

Figure 14. 1σ uncertainty regions for the binarity fraction as a function of KOI period for two different planetary populations, with only companions with separations $<2\farcs5$ used to align with Paper I.

5.3.4. Stellar Multiplicity and Close-in Planets Revisited

The presence of stellar companions is hypothesized to shape the formation and evolution of planetary systems. Overall, there is evidence that planetary formation is disrupted in close binary systems (Fragner et al. 2011; Roell et al. 2012). The third body in the system can lead to Kozai oscillations causing orbital migration of the planets (Fabrycky & Tremaine 2007; Katz et al. 2011; Naoz et al. 2012) or tilt the circumstellar disk (Batygin 2012). Smaller planets are also more prone to the influence of a stellar companion because of weaker planet-planet dynamical coupling (Wang et al. 2015a). These dynamical interactions between small and large planets in the same system tend to differentially eject small planets more frequently than large planets (Xie et al. 2014). The presence of a stellar companion increases the frequency of these interactions, leading to higher loss of small planets. Consequently, we would expect a correlation between binarity and planetary period for different sized planets.

We previously reported a low-significance result of stellar third bodies increasing the rate of close-in giant planets, possible evidence of orbital migration of the planet caused by the stellar companion. We revisit the discussion and analysis from Paper I in search of this correlation using the results of Paper II and this work. This analysis splits the "small" and "giant" planets at the arbitrary value of Neptune's radius ($3.9R_{\oplus}$). The exact value does not significantly affect the results, as just 11 of the detected systems have planetary radii within 20% of the cutoff value, with 1635 small and 395 giant planets in total.

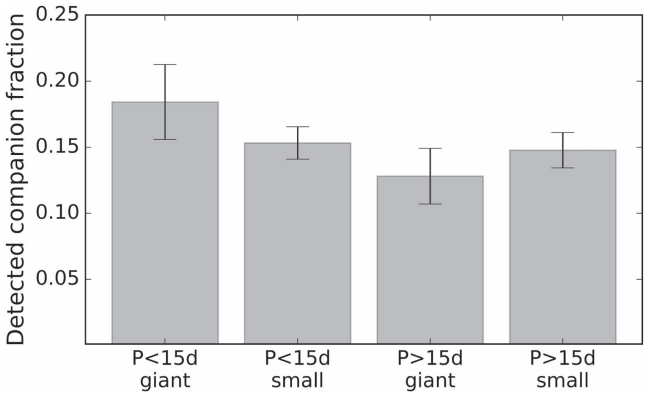

Figure 15. Multiplicity fraction of KOIs with four planetary populations, with all contrast ratios and separations $\leqslant 4''$. A planet is considered giant if its radius is equal to or larger to that of Neptune ($3.9\ R_{\oplus}$). Multi-planet systems can be assigned to multiple populations.

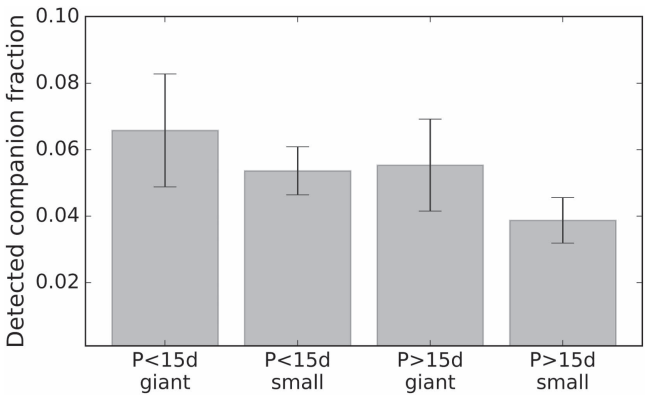

Figure 16. Multiplicity fraction of KOIs with four planetary populations, with only companions with $\Delta m \leqslant 2$ and separations $\leqslant 1\farcs5$, removing the faint nearby stars that are less likely to be physically associated.

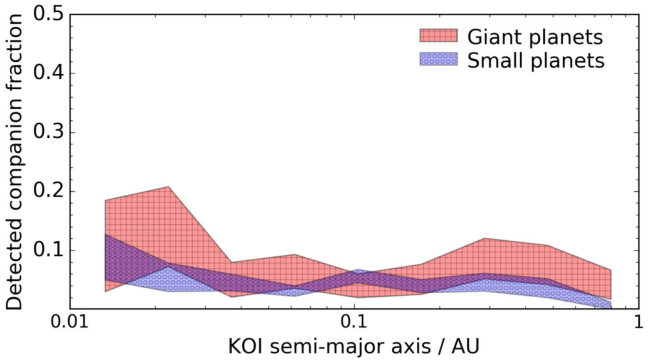

Figure 17. 1σ uncertainty regions for the binarity fraction as a function of KOI semimajor axis between 0.01 and 1.0 AU for two different planetary populations.

In Figure 13, the fraction of *Kepler* planet candidates with nearby stars is shown, with planets grouped into two different size ranges. We again see a small increase in the nearby star fraction for giants with periods <15 days; however, the $>2\sigma$ spike at periods of 2–4 days seen in Paper I is not present. If our sample is reduced to correspond to the separation range of Paper I ($\rho < 2\farcs5$) in Figure 14, again no binarity spike at periods <10 days is apparent.

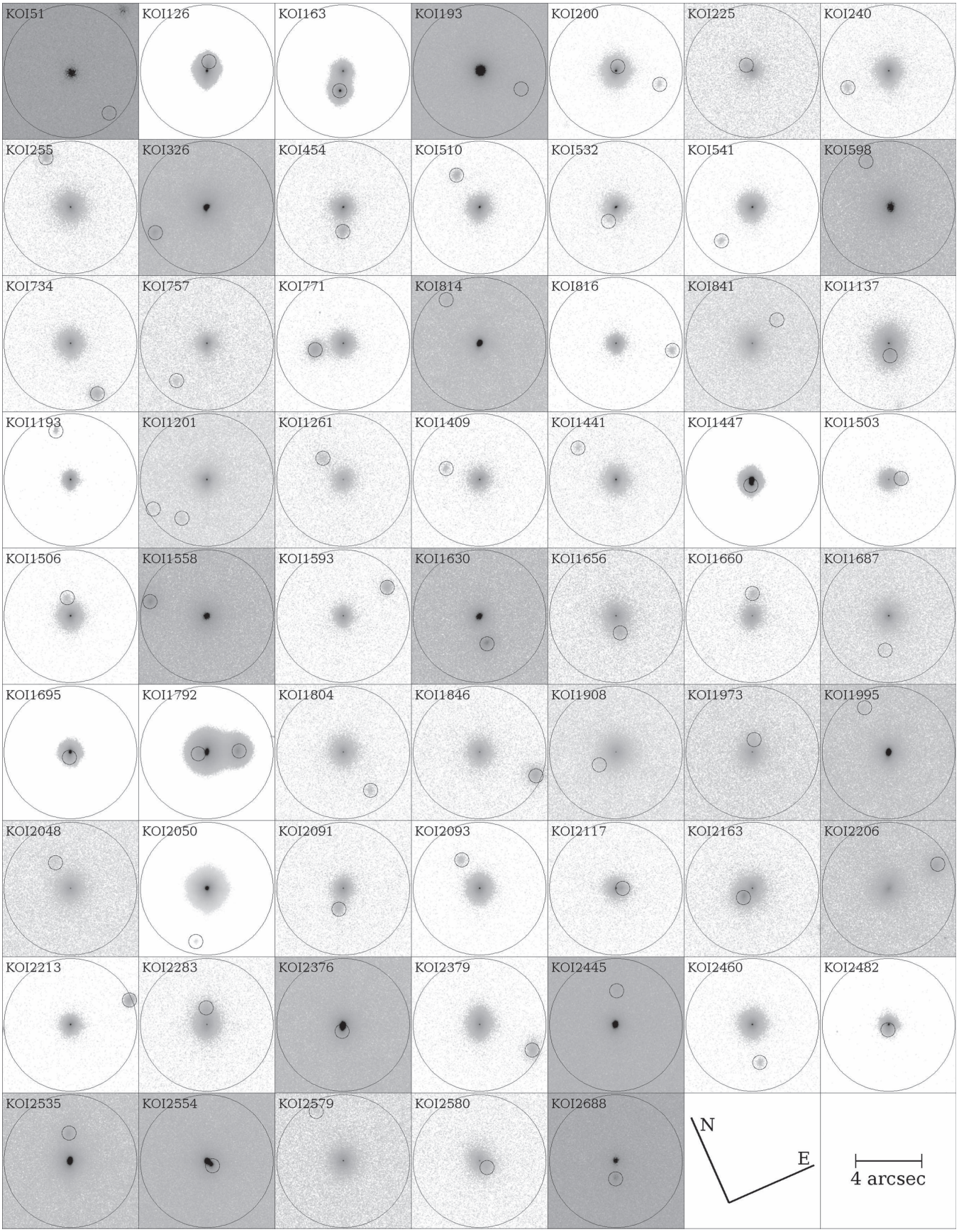

Figure 18. Color-inverted, normalized log-scale cutouts of 61 multiple KOI systems [KOI-51 to KOI-2688] with separations $<4''$ resolved with Robo-AO. The angular scale and orientation is similar for each cutout. The smaller circles are centered on the detected nearby star, and the larger circle is the limit of the survey's $4''$ separation range.

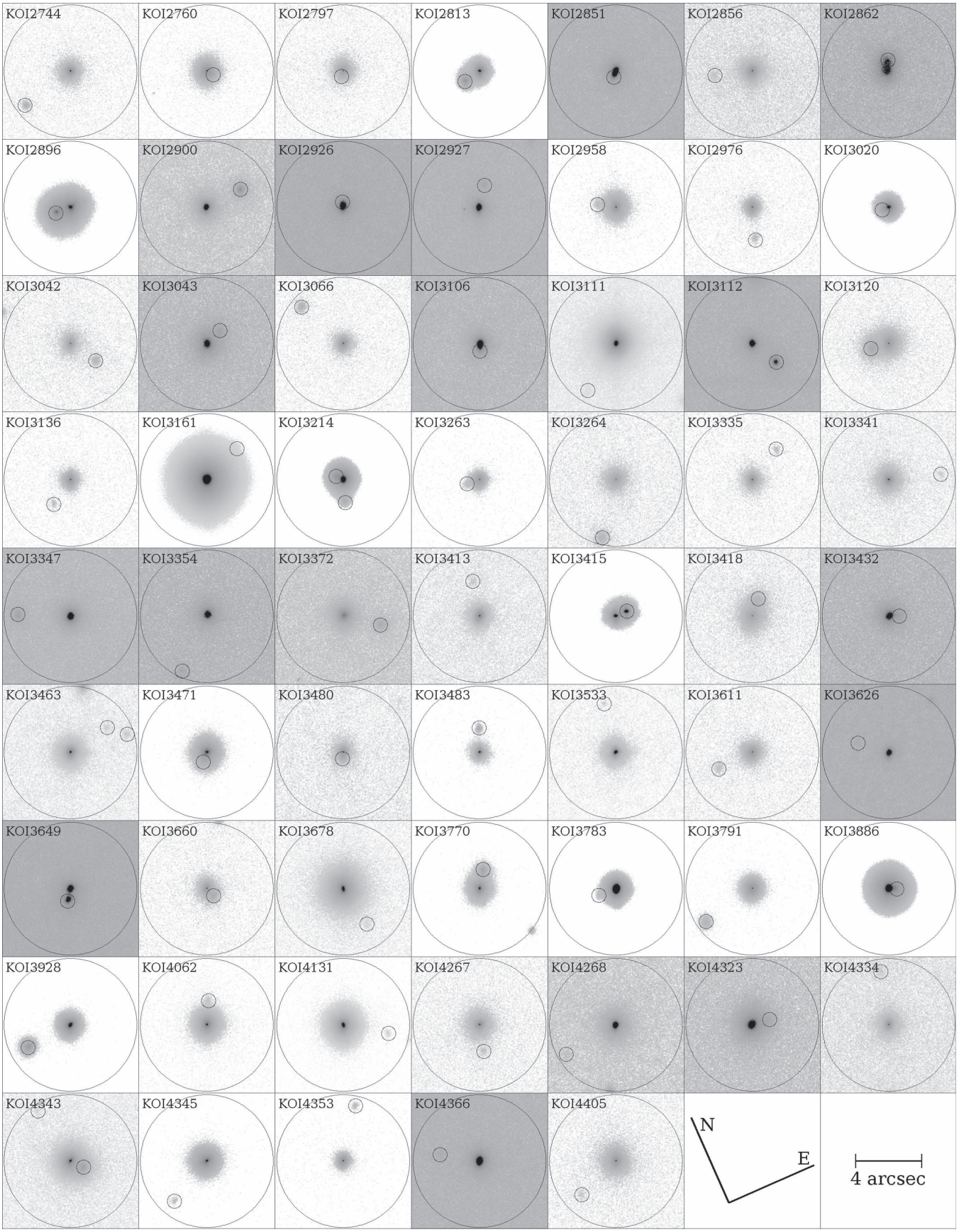

Figure 19. Color-inverted, normalized log-scale cutouts of 61 multiple KOI systems [KOI-2744 to KOI-4405], with separations $<4''$ resolved with Robo-AO. The angular scale and orientation is similar for each cutout. The smaller circles are centered on the detected nearby star, and the larger circle is the limit of the survey's $4''$ separation range.

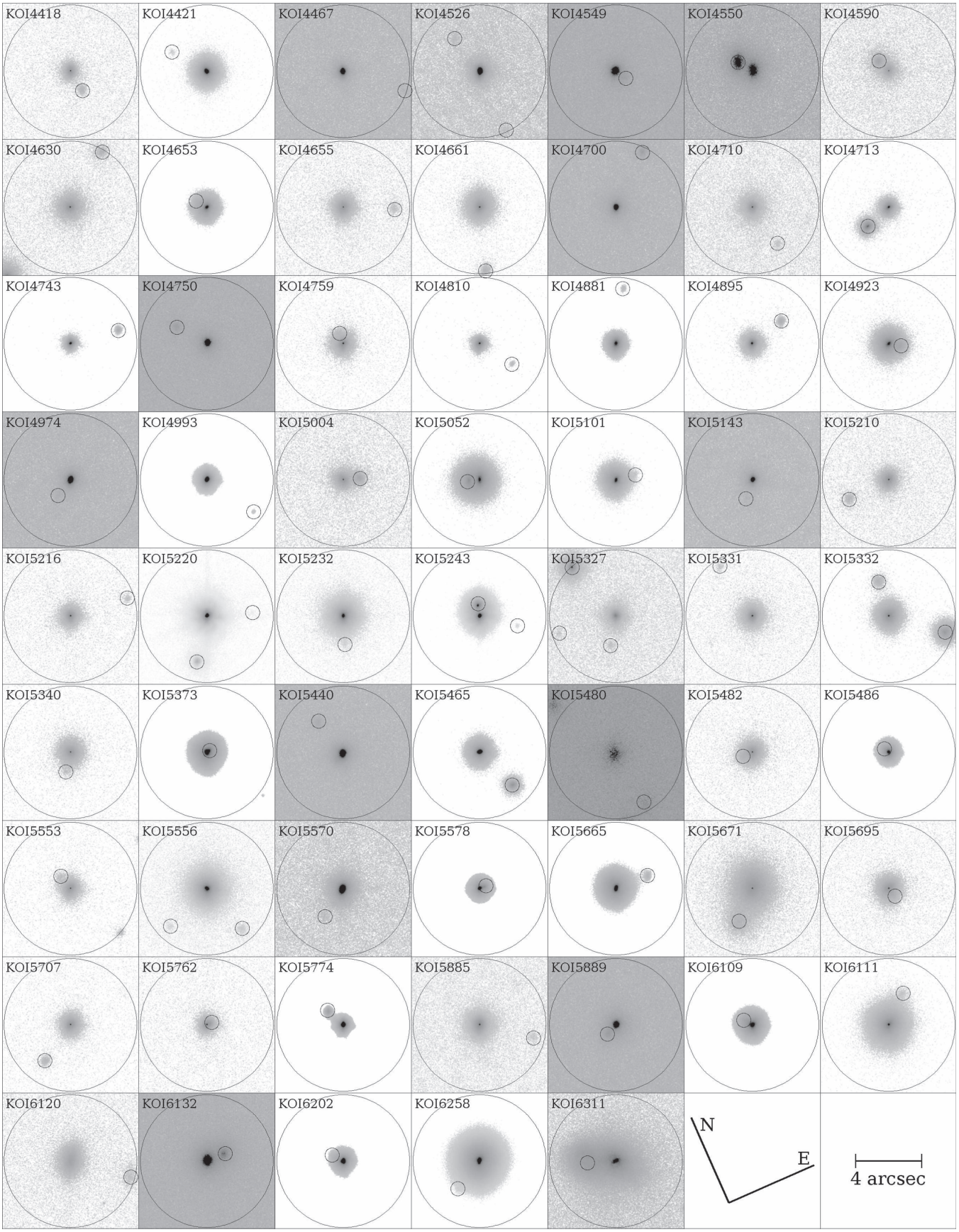

Figure 20. Color-inverted, normalized log-scale cutouts of 61 multiple KOI systems [KOI-4418 to KOI-6311] with separations $<4''$ resolved with Robo-AO. The angular scale and orientation is similar for each cutout. The smaller circles are centered on the detected nearby star, and the larger circle is the limit of the survey's $4''$ separation range.

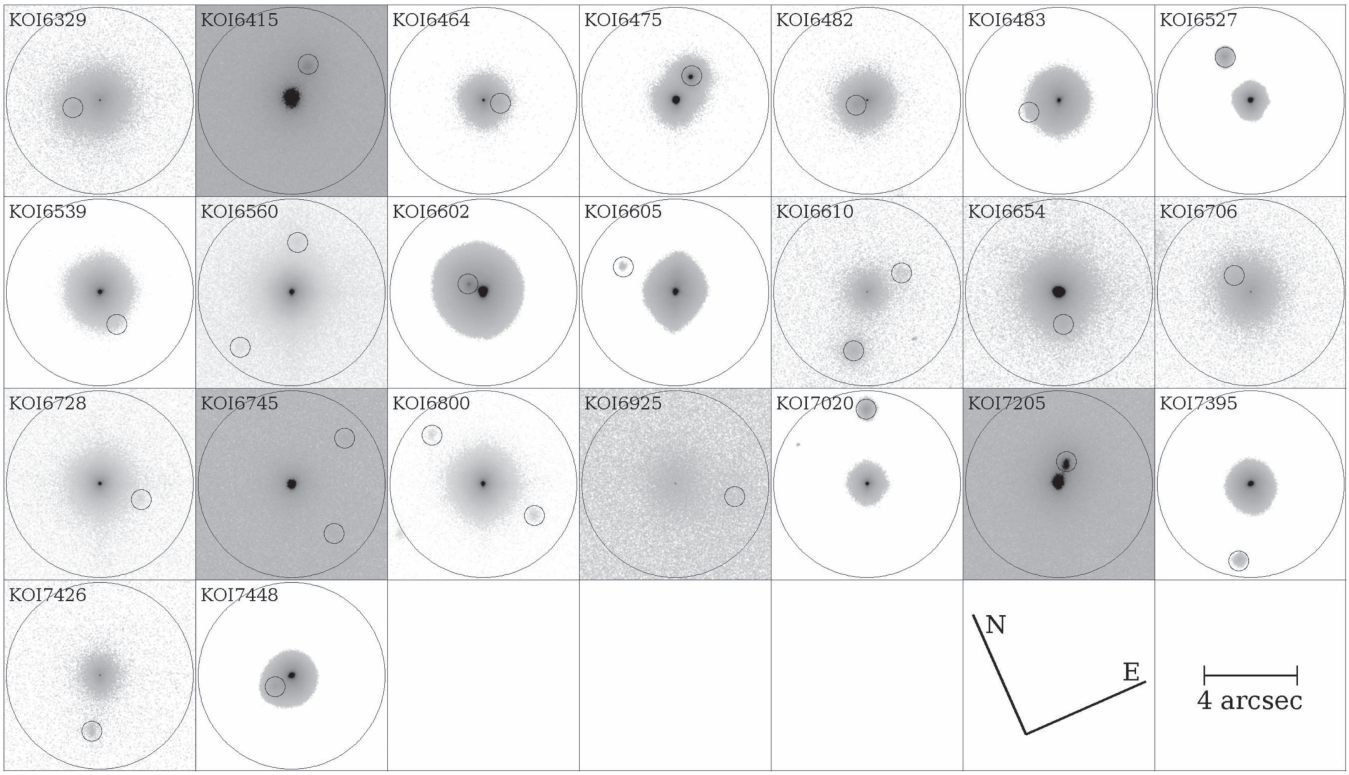

Figure 21. Color-inverted, normalized log-scale cutouts of 23 multiple KOI systems [KOI-6329 to KOI-7448] with separations $<4''$ resolved with Robo-AO. The angular scale and orientation is similar for each cutout. The smaller circles are centered on the detected nearby star, and the larger circle is the limit of the survey's $4''$ separation range.

Binning our targets into four population groups in Figure 15 suggests no significant difference in the binarity rate of short period giants. We also attempt to decrease the occurrence of unassociated asterisms by only using close, bright companions ($\Delta m \leqslant 2$, $\rho \leqslant 1\farcs5$). As in Paper I, we detected an excess of close-separation bright companions (Figure 5), which suggests a higher probability of association for these nearby stars. We show the binarity fraction of the four populations in Figure 16. As with the complete set of nearby stars, no significant differences between the four populations is evident.

Any real disparity between the populations would also manifest in the physical orbital semimajor axis, which is related to the observable periods by the stellar mass. In Figure 17, we plot the two population's binarity fraction as a function of the calculated semimajor axis of the planetary candidates between 0.01 and 1.0 AU. No significant giant planet binarity spike is observed, as in the periods plot.

Our updated study, using the targets in Paper II and this work, suggests that the presence of a second stellar body in planetary systems does not appreciably affect the number of close-in giant planets. This agrees with the analysis of Wang et al. (2015a), who find a relatively uniform multiplicity rate for planets with short and long periods. They note that our previous tentative result may have been due to short-period giants with brighter stellar companions in the visible biasing our detections. Subject to the same potential biases, the larger survey in this analysis does not indicate a period-multiplicity correlation for the two planetary populations, suggesting that our previous low-sigma result may have instead been an artifact of small-number statistics.

Kraus et al. (2016) find a 6.6σ deficit in binary stars with separation $\rho < 50$ AU in KOIs, compared to field stars, again suggesting that close-in stellar companions disrupt the formation and/or evolution of planets, as had been previously hypothesized (Wang et al. 2014). Indeed, a quarter of all solar-type stars in the Milky Way are disallowed from hosting planetary systems due to the influence of binary companions.

Some evidence remains, however, that stellar binarity may encourage the presence of hot Jupiters. A recent NIR survey (Ngo et al. 2015) of exoplanetary systems with known close-in giants finds that hot Jupiter hosts are twice as likely as field stars to be found in a multiple star system, with a significance of 2.8σ. However, the binarity rates of systems containing hot Jupiters remains unclear: 12% (Roell et al. 2012), 38% (Evans et al. 2016), 51% (Ngo et al. 2015).

We will revisit this discussion in the last paper of this series, where we will combine the full Robo-AO KOI survey data set.

6. CONCLUSION

We observed 1629 *Kepler* planetary candidates with the Robo-AO robotic laser adaptive optics system. We detected 206 planetary candidates with nearby stars, implying an overall nearby-star probability of $12.6\% \pm 0.9\%$ at separations between $\sim 0\farcs15$ and $4\farcs0$ and $\Delta m \leqslant 6$.

Many of our newly found companions are of particular interest, including 26 habitable zone candidates found within possible multiple star systems. In addition, we found 16 KOIs with multiple nearby stars, and five new candidate quadruple star systems hosting planet candidates, including KOI-4495 from Paper II. We looked at broad correlations between the presence of nearby stars and planetary characteristics. We find a higher detected companion rate of systems with multiple planets than in single planet systems. Our previous tentative

result of a deficit of close-in giant planets when a third stellar body appears in the system is not apparent in this data set.

The Robo-AO system was installed on the 2.1 m telescope at Kitt Peak in 2015 November, and a new low-noise infrared camera that will allow observations of redder companion stars will be added in the future. In addition, a second-generation Robo-AO instrument on the University of Hawai'i 2.2 m telescope on Maunakea (Baranec et al. 2014a) is being built. The two systems will together image up to ~500 objects per night and have access to three-quarters of the sky over the course of a year. A southern analog to Robo-AO, mounted on the Southern Astrophysical Research Telescope (SOAR) at CTIO and capable of twice *HST* resolution imaging, is also in development. With unmatched efficiency, Robo-AO and its lineage of instruments are uniquely able to perform high-acuity imaging of the hundreds of K2 (Howell et al. 2014) planetary candidates, ground-based transit surveys such as MEarth (Nutzman & Charbonneau 2008), KELT (Pepper et al. 2007, 2012), HATNet (Bakos et al. 2004), SuperWASP (Pollacco et al. 2006), NGTS (Wheatley et al. 2013), XO (McCullough et al. 2005), and the Evryscope (Law et al. 2015), as well as the thousands of expected exoplanet hosts discovered by the forthcoming NASA Transiting Exoplanet Survey Satellite (TESS, Ricker et al. 2015) and ESA PLAnetary Transits and Oscillations of stars 2.0 (PLATO, Rauer et al. 2014) missions.

The Robo-AO survey has completed observations of over 90% of the *Kepler* planet candidates, with the remaining targets to be observed at the Kitt Peak telescope. Future papers in this survey will present these final KOI targets, and perform a full probability of association analysis. With the entire survey soon to be completed, providing us with an unprecedented data set of thousands of high angular resolution imaged planetary candidates, we can continue our search for clues to planetary formation and evolution.

We thank the anonymous referee for careful analysis and useful comments on the manuscript.

This research is supported by the NASA Exoplanets Research Program, grant #NNX 15AC91G. C.B. acknowledges support from the Alfred P. Sloan Foundation. T.M. is supported by NASA grant #NNX 14AE11G under the Kepler Participating Scientist Program. D.A. is supported by a NASA Space Technology Research Fellowship, grant #NNX 13AL75H.

The Robo-AO system is supported by collaborating partner institutions, the California Institute of Technology, the Inter-University Centre for Astronomy and Astrophysics, the National Science Foundation under Grant Nos. AST-0906060, AST-0960343, and AST-1207891, the Mount Cuba Astronomical Foundation, and by a gift from Samuel Oschin. We are grateful to the Palomar Observatory staff for their ongoing support of Robo-AO on the 1.5 m telescope, particularly S. Kunsman, M. Doyle, J. Henning, R. Walters, G. Van Idsinga, B. Baker, K. Dunscombe, and D. Roderick.

Some of the data presented herein were obtained at the W.M. Keck Observatory, which is operated as a scientific partnership among the California Institute of Technology, the University of California, and the National Aeronautics and Space Administration. The Observatory was made possible by the generous financial support of the W.M. Keck Foundation. Some of the data presented herein is based on observations obtained at the Gemini Observatory, operated by the Association of Universities for Research in Astronomy, Inc., under a cooperative agreement with the NSF on behalf of the Gemini partnership. We recognize and acknowledge the very significant cultural role and reverence that the summit of Maunakea has always had within the indigenous Hawaiian community. We are most fortunate to have the opportunity to conduct observations from this mountain.

We thank Adam Kraus et al. for sharing a preprint of their paper.

This research has made use of the SIMBAD database, operated by Centre des Données Stellaires (Strasbourg, France), and bibliographic references from the Astrophysics Data System maintained by SAO/NASA. This research has made use of the *Kepler* Community FollowUp Observing Program Web site (https://cfop.ipac.caltech.edu) and the NASA Exoplanet Archive, which is operated by the California Institute of Technology, under contract with the National Aeronautics and Space Administration under the Exoplanet Exploration Program. This work used the K2fov (Mullally & Barclay 2016) Python package.

Facilities: PO:1.5m (Robo-AO), Keck:II (NIRC2-LGS), Gemini:Gillett (NIRI).

APPENDIX

In Table 9, we list our Robo-AO observed KOIs, including date the target was observed, observation quality (as described in Section 3.6), the estimated latest detectable companion spectral type (as described in Section 3.7.3), and the presence of detected companions.

Table 9
Full Robo-AO Observation List

KOI	m_i (mag)	ObsID	Filter	Obs. Qual.	Latest Det. Comp. SpT	Comp. Det.?
K020	13.29	2014 Aug 22	i'	medium	M4	
K051	14.48	2013 Jul 25	LP600	medium	M4	yes
K076	10.05	2014 Aug 22	i'	high	M4	
K0104	12.78	2014 Aug 22	i'	medium	M6	
K0126	13.11	2015 Jun 08	LP600	high	M5	yes
K0134	15.02	2012 Jul 16	i'	medium	M4	
K0135	13.8	2012 Jul 17	i'	low	M1	
K0163	13.3	2012 Jul 18	LP600	high	M6	yes
K0186	14.76	2014 Aug 31	LP600	medium	M4	
K0193	14.9	2014 Aug 21	LP600	high	M4	yes

(This table is available in its entirety in machine-readable form.)

REFERENCES

Adams, E. R., Ciardi, D. R., Dupree, A. K., et al. 2012, AJ, 144, 42
Adams, E. R., Dupree, A. K., Kulesa, C., & McCarthy, D. 2013, AJ, 146, 9
Atkinson, D., Baranec, C., Ziegler, C., et al. 2017, AJ, 153, 25
Bakos, G., Noyes, R. W., Kovács, G., et al. 2004, PASP, 116, 266
Baranec, C., Riddle, R., Law, N. M., et al. 2013, Journal of Visualized Experiments, 72, e50021
Baranec, C., Riddle, R., Law, N. M., et al. 2014a, Proc. SPIE, 9148, 914812
Baranec, C., Riddle, R., Law, N. M., et al. 2014b, ApJL, 790, L8
Baranec, C., Ziegler, C., Law, N. M., et al. 2016, AJ, 152, 18
Barclay, T., Quintana, E. V., Adams, F. C., et al. 2015, ApJ, 809, 7
Batalha, N. M., Borucki, W. J., Koch, D. G., et al. 2010, ApJL, 713, L109
Batalha, N. M., Rowe, J. F., Bryson, S. T., et al. 2013, ApJS, 204, 24
Batygin, K. 2012, Natur, 491, 418
Borucki, W. J., Koch, D. G., Basri, G., et al. 2011a, ApJ, 728, 117
Borucki, W. J., Koch, D. G., Basri, G., et al. 2011b, ApJ, 736, 19
Borucki, W. J., Koch, D. G., Brown, T. M., et al. 2010, ApJL, 713, L126
Brown, T. M., Latham, D. W., Everett, M. E., & Esquerdo, G. A. 2011, AJ, 142, 112
Burgasser, A. J., Kirkpatrick, J. D., Reid, I. N., et al. 2003, ApJ, 586, 512
Burke, C. J., Bryson, S. T., Mullally, F., et al. 2014, ApJS, 210, 19
Ciardi, D. R., Beichman, C. A., Horch, E. P., & Howell, S. B. 2015, ApJ, 805, 16
Ciardi, D. R., von Braun, K., Bryden, G., et al. 2011, AJ, 141, 108
Désert, J.-M., Charbonneau, D., Torres, G., et al. 2015, ApJ, 804, 59
Dressing, C. D., Adams, E. R., Dupree, A. K., Kulesa, C., & McCarthy, D. 2014, AJ, 148, 78
Dressing, C. D., & Charbonneau, D. 2013, ApJ, 767, 95
Duchêne, G., & Kraus, A. 2013, ARA&A, 51, 269
Duquennoy, A., & Mayor, M. 1991, A&A, 248, 485
Evans, D. F., Southworth, J., Maxted, P. F. L., et al. 2016, A&A, 589, 58
Everett, M. E., Barclay, T., Ciardi, D. R., et al. 2015, AJ, 149, 55
Fabrycky, D., & Tremaine, S. 2007, ApJ, 669, 1298
Fabrycky, D. C., Ford, E. B., Steffen, J. H., et al. 2012, ApJ, 750, 114
Fragner, M. M., Nelson, R. P., & Kley, W. 2011, A&A, 528, A40
Fressin, F., Torres, G., Charbonneau, D., et al. 2013, ApJ, 766, 81
Fruchter, A. S., & Hook, R. N. 2002, PASP, 114, 144
Gilliland, R. L., Cartier, K. M. S., Adams, E. R., et al. 2015, AJ, 149, 24
Gross, E., & Vitells, O. 2010, EPJC, 70, 525
Haas, M. R., Batalha, N. M., Bryson, S. T., et al. 2010, ApJL, 713, L115
Heller, R. 2012, A&A, 545, L8
Hodapp, K. W., Jensen, J. B., Irwin, E. M., et al. 2003, PASP, 115, 1388
Horch, E. P., Howell, S. B., Everett, M. E., & Ciardi, D. R. 2012, AJ, 144, 165
Horch, E. P., Howell, S. B., Everett, M. E., & Ciardi, D. R. 2014, ApJ, 795, 60
Howell, S. B., Everett, M. E., Sherry, W., Horch, E., & Ciardi, D. R. 2011, AJ, 142, 19
Howell, S. B., Sobeck, C., Haas, M., et al. 2014, PASP, 126, 398
Kasting, J. F., Whitmire, D. P., & Reynolds, R. T. 1993, Icar, 101, 108
Katz, B., Dong, S., & Malhotra, R. 2011, PhRvL, 107, 181101
Kolbl, R., Marcy, G. W., Isaacson, H., & Howard, A. W. 2015, AJ, 149, 18
Kraus, A. L., & Hillenbrand, L. A. 2007, AJ, 134, 2340
Kraus, A. L., Ireland, M. J., Huber, D., Mann, A. W., & Dupuy, T. J. 2016, AJ, 152, 8
Lafrenière, D., Marois, C., Doyon, R., Nadeau, D., & Artigau, É. 2007, ApJ, 660, 770
Law, N. M., Fors, O., Ratzloff, J., et al. 2015, PASP, 127, 234
Law, N. M., Mackay, C. D., Dekany, R. G., et al. 2009, ApJ, 692, 924
Law, N. M., Morton, T., Baranec, C., et al. 2014, ApJ, 791, 35
Lawrence, A., Warren, S. J., Almaini, O., et al. 2007, MNRAS, 379, 1599
Lillo-Box, J., Barrado, D., & Bouy, H. 2012, A&A, 546, A10
Lillo-Box, J., Barrado, D., & Bouy, H. 2014, A&A, 566, A103
Lissauer, J. J., Dawson, R. I., & Tremaine, S. 2014, Natur, 513, 336
Marcy, G. W., Isaacson, H., Howard, A. W., et al. 2014, ApJS, 210, 20
McCullough, P. R., Stys, J. E., Valenti, J. A., et al. 2005, PASP, 117, 783
Morton, T. D., Bryson, S. T., Coughlin, J. L., et al. 2016, ApJ, 822, 86
Morton, T. D., & Johnson, J. A. 2011, ApJ, 738, 170
Mullally, F., & Barclay, T. B. G. 2016, K2fov: Field of view software for NASA's K2 mission, ascl:1601.009
Mullally, F., Coughlin, J. L., Thompson, S. E., et al. 2015, ApJS, 217, 31
Naoz, S., Farr, W. M., & Rasio, F. A. 2012, ApJL, 754, L36
Ngo, H., Knutson, H. A., Hinkley, S., et al. 2015, ApJ, 800, 138
Nutzman, P., & Charbonneau, D. 2008, PASP, 120, 317
Pepper, J., Kuhn, R. B., Siverd, R., James, D., & Stassun, K. 2012, PASP, 124, 230
Pepper, J., Pogge, R. W., DePoy, D. L., et al. 2007, PASP, 119, 923
Pickles, A. J. 1998, PASP, 110, 863
Pollacco, D. L., Skillen, I., Collier Cameron, A., et al. 2006, PASP, 118, 1407
Raghavan, D., McAlister, H. A., Henry, T. J., et al. 2010, ApJS, 190, 1
Rasio, F. A., & Ford, E. B. 1996, Sci, 274, 954
Rauer, H., Catala, C., Aerts, C., et al. 2014, ExA, 38, 249
Ricker, G. R., Winn, J. N., Vanderspek, R., et al. 2015, JATIS, 1, 014003
Riddle, R. L., Burse, M. P., Law, N. M., et al. 2012, Proc. SPIE, 8447, 2
Roberts, L. C., Jr., Tokovinin, A., Mason, B. D., et al. 2015, AJ, 149, 118
Roell, T., Neuhäuser, R., Seifahrt, A., & Mugrauer, M. 2012, A&A, 542, A92
Rogers, L. A. 2015, ApJ, 801, 41
Rowe, J. F., Bryson, S. T., Marcy, G. W., et al. 2014, ApJ, 784, 45
Santerne, A., Díaz, R. F., Moutou, C., et al. 2012, A&A, 545, A76
Santerne, A., Fressin, F., Díaz, R. F., et al. 2013, A&A, 557, A139
Santerne, A., Moutou, C., Tsantaki, M., et al. 2016, A&A, 587, 64
Schwamb, M. E., Orosz, J. A., Carter, J. A., et al. 2013, ApJ, 768, 127
Seager, S. 2013, Sci, 340, 577
Selsis, F., Kasting, J. F., Levrard, B., et al. 2007, A&A, 476, 1373
Skrutskie, M. F., Cutri, R. M., Stiening, R., et al. 2006, AJ, 131, 1163
Thompson, S. E., Mullally, F., Coughlin, J., et al. 2015, ApJ, 812, 46
Torres, G., Kipping, D. M., Fressin, F., et al. 2015, ApJ, 800, 99
van Dam, M. A., Bouchez, A. H., Le Mignant, D., et al. 2006, PASP, 118, 310
Wang, J., Fischer, D. A., Horch, E. P., & Xie, J.-W. 2015a, ApJ, 806, 248
Wang, J., Fischer, D. A., Xie, J.-W., & Ciardi, D. R. 2014, ApJ, 791, 111
Wang, J., Fischer, D. A., Xie, J.-W., & Ciardi, D. R. 2015b, ApJ, 813, 130
Wheatley, P. J., Pollacco, D. L., Queloz, D., et al. 2013, European Physical Journal Web of Conferences, 47, 13002
Wizinowich, P., Acton, D. S., Shelton, C., et al. 2000, PASP, 112, 315
Wizinowich, P. L., Le Mignant, D., Bouchez, A. H., et al. 2006, PASP, 118, 297
Xie, J.-W., Wu, Y., & Lithwick, Y. 2014, ApJ, 789, 165
Yelda, S., Lu, J. R., Ghez, A. M., et al. 2010, ApJ, 725, 331
Ziegler, C., Law, N. M., Baranec, C., Riddle, R. L., & Fuchs, J. T. 2015, ApJ, 804, 30
Zsom, A., Seager, S., de Wit, J., & Stamenković, V. 2013, ApJ, 778, 109